



## UvA-DARE (Digital Academic Repository)

### Towards improved source apportionment of organic matter in soil and peat using lipid biomarkers and inverse modeling

Thomas, C.L.

**Publication date**  
2024

[Link to publication](#)

#### **Citation for published version (APA):**

Thomas, C. L. (2024). *Towards improved source apportionment of organic matter in soil and peat using lipid biomarkers and inverse modeling*. [Thesis, fully internal, Universiteit van Amsterdam, Universität Zürich, Zürich, Switzerland].

#### **General rights**

It is not permitted to download or to forward/distribute the text or part of it without the consent of the author(s) and/or copyright holder(s), other than for strictly personal, individual use, unless the work is under an open content license (like Creative Commons).

#### **Disclaimer/Complaints regulations**

If you believe that digital publication of certain material infringes any of your rights or (privacy) interests, please let the Library know, stating your reasons. In case of a legitimate complaint, the Library will make the material inaccessible and/or remove it from the website. Please Ask the Library: <https://uba.uva.nl/en/contact>, or a letter to: Library of the University of Amsterdam, Secretariat, P.O. Box 19185, 1000 GD Amsterdam, The Netherlands. You will be contacted as soon as possible.

EVALUATING THE APPLICABILITY OF THE VERHIB MODEL  
TO A 2600-YEAR PEAT SEQUENCE FROM CENTRAL  
GERMANY

Carrie L. Thomas<sup>1,2</sup>, Boris Jansen<sup>2</sup>, E. Emiel van Loon<sup>2</sup>, Guido L. B. Wiesenberg<sup>1</sup>

<sup>1</sup>Department of Geography, University of Zurich, 8057 Zurich, Switzerland

<sup>2</sup>Institute for Biodiversity and Ecosystem Dynamics, University of Amsterdam, Amsterdam, 1098XH, The Netherlands

Planned to submit to *Palaeogeography, Palaeoclimatology, Palaeoecology*.

## ABSTRACT

Organic matter stored in soil and peat is the largest terrestrial carbon sink and, therefore, an important component of the global carbon cycle. To enable increased carbon sequestration, it is vital to close gaps in the understanding of soil organic matter incorporation, formation, and degradation processes. Reconstructing paleovegetation is one approach that can improve source apportionment of organic matter, allowing for the enhanced process understanding necessary for optimization of soil carbon pools. Additionally, paleovegetation reconstruction can be used to improve climate-vegetation links in existing climate models and forecast future changes in vegetation patterns. Plant-derived biomarkers have been used extensively for source identification in soil, peat, and sediments. However, using biomarkers for vegetation reconstruction can be complicated because individual compounds do not indicate specific plant sources. The composition across multiple compounds must be holistically evaluated to develop accurate reconstructions. The VERHIB model was developed to enable a range of *n*-alkane and *n*-alkanol data to be evaluated simultaneously and estimate past vegetation development using the biomarker signature of leaves and roots from modern plants compared to the preserved, mixed signature of a soil or peat core. In this study, we have applied the VERHIB model to data gathered from the Beerberg peatland in Central Germany. A previous study characterized plant macrofossils, pollen, *n*-alkane, *n*-alkanol, and *n*-fatty acid composition in the Beerberg peat. We have collected modern plant samples from the peatland and measured their biomarker composition to use as input for the model. Despite many overlapping biomarker signatures across plant species and parts, our results shows that the model could recreate a reasonable vegetation development pattern for most of the peat core if *n*-fatty acid data was included alongside *n*-alkane data. The model had difficulty recreating the transition from poor fen vegetation to *Sphagnum* bog, which was evident in the plant macrofossil records, so further calibration is needed. This was the first attempt at considering *n*-fatty acid data in a reconstruction using the VERHIB model; previous reconstructions only included *n*-alkanes or a combination of *n*-alkanes and *n*-alkanols. Our study shows that *n*-fatty acids are a valuable compound class to add to the VERHIB model and provides recommendations for future development.

## INTRODUCTION

Soil organic matter (SOM) is a key carbon sink in the global carbon cycle, storing about four times the amount of carbon (1700 PgC) as the entire stock of terrestrial vegetation (450 PgC) (Erb et al., 2018; Jackson et al., 2017). To combat climate change, it is imperative to protect and optimize this sink to reduce the amount of carbon in the atmosphere. Pursuant to that goal, it is essential to gain a deeper understanding of how soil organic matter is formed and subsequently cycles (Schmidt et al., 2011). Better identification of the sources of organic matter in soil could aid in improved process understanding and potential regulation of these processes to enable increased carbon sequestration. As the remains of past vegetation are the primary contributor to organic matter in soil, reconstructing vegetation development through time is one way to identify sources of SOM. Furthermore, vegetation reconstruction provides insight into past climate patterns and can be used to improve climate models and predict how ecosystems will respond to climate change (Lavorel et al., 2007). This is especially true in the case of vegetation reconstructions that do not include climate data as input or boundary conditions.

One tool used extensively for source identification in lacustrine and marine sediments, as well as soil and peat archives, is "molecular fossils" or biomarkers (Peters et al., 2005). These are chemical components of previous life forms that are preferentially preserved following deposition. Many biomarkers have also been connected to specific sources, particularly those derived from plant waxes: long-chain *n*-alkanes, *n*-alkanols, and *n*-fatty acids. Numerous studies have identified specific concentration patterns that have allowed for past vegetation shifts to be determined. However, single compounds are not indicative of individual plant sources, and interpreting the data requires holistically considering the biomarkers across a range of chain lengths (Jansen et al., 2006, 2010). It can be challenging to assess the data and untangle individual sources as well as to draw robust conclusions concerning past environmental changes.

Additionally, biomarkers are present not only in leaves but also in other plant organs, including roots, which typically have a different chemical composition (e.g., Jansen et al., 2006). This can obscure the process of source apportionment due to the overlap in chemical signatures of aboveground and belowground biomass and the potential for belowground

biomass to overprint the signature of previously incorporated aboveground biomass, specifically in deeper soil horizons (Gocke et al., 2010; Lavrieux et al., 2012). Further, many potential climatic, environmental, and developmental variables can affect the biomarker composition of plant waxes. Therefore, the biomarker signature measured at one location of a species may be very different from that of the same species in another environment or even in a different growth stage (Jansen and Wiesenberg, 2017). Recent studies highlight the continuous incorporation of plant wax components into soils, as opposed to only from litterfall, which points to the need to further disentangle the incorporation pathways of organic matter into soil (Srivastava and Wiesenberg, 2018). Despite these uncertainties regarding incorporation and source assessment of organic matter in soils, the degradation continuum of wax biomarkers from fresh plant biomass via organic horizons toward mineral soil still highlights the robustness of the approach that vegetation composition is reflected in mineral soils through the biomarker composition, and this consequently enables source apportionment of soil organic matter (Hirave et al., 2020; Thomas et al., 2021).

The Vegetation Reconstruction with the Help of Inverse modeling and Biomarkers (VERHIB) model was developed to make deciphering biomarker data easier and enable more quantitative interpretations (Jansen et al., 2010). The model was developed using MATLAB and includes *n*-alkanes and *n*-alkanols. A forward model calculates the accumulated mass of biomarkers per archive depth layer using annual biomass production per plant species as input and the biomarker composition of plant leaves and roots, the distribution over depth of plant roots and leaves, and the partitioning of biomass over plant leaves and roots as parameters. The forward model is then inverted to solve for the proportion of biomarkers that each plant species contributes per depth layer, serving as an estimate of the vegetation composition through time (Jansen et al., 2010). This output provides an assessment of vegetation composition similar to that of pollen or macrofossil data. However, due to the preferential degradation of plant remains, including pollen and macrofossils, in oxic environments, the more recalcitrant molecular fossils can provide more reasonable output in contexts where there is a severely degraded pollen or macrofossil record, such as terrestrial sediments like loess-paleosol sequences. The molecular marker-based VERHIB model has already been applied successfully in a handful of locales, including the Andes using both peat and soil cores (Jansen et al., 2010, 2013) and further

investigated in other archives, such as polycyclic driftsand sequences (Van Mourik & Jansen, 2013) and plaggic Anthrosols (Van Mourik et al., 2016).

Previously, we investigated the Beerberg peatland in Thuringia, Germany using high-resolution biomarker, pollen, and macrofossil data (Thomas et al., 2023a). Although there was a short period of drainage in the past, the Beerberg peatland has been under protection for decades and is, therefore, relatively undisturbed. Additionally, we were able to establish a robust age-depth model, and having the pollen and macrofossil data available will allow us to better determine whether a reconstruction using VERHIB is credible. Earlier work with the VERHIB model had lower-resolution biomarker data and only pollen records available for comparison. Furthermore, the VERHIB model has yet to be applied using *n*-fatty acid data. Prior studies incorporating the VERHIB model have either used only *n*-alkane data (Van Mourik et al., 2016) or a combination of *n*-alkane and *n*-alkanol data (Jansen et al., 2010, 2013; Van Mourik & Jansen, 2013).

Therefore, the objectives of this study were to

- (a) establish a reference library of plant biomarker signatures (*n*-alkanes, *n*-alkanols, *n*-fatty acids) at Beerberg peatland,
- (b) apply the VERHIB model to the biomarker data from the Beerberg peatland including the *n*-fatty acid composition, and compare it to the previously completed multi-proxy analysis of the Beerberg peatland development, and
- (c) evaluate the sensitivity of the VERHIB result across a range of parameter choices.

## MATERIALS AND METHODS

### STUDY SITE AND SAMPLING

The Beerberg peatland (50°39'32" N, 10°44'36" E, 983 m) is an ombrotrophic peat bog atop the Grosser Beerberg and is part of the Vessertal-Thuringian Forest Biosphere Reserve in central Germany. In October 2019, we took core samples of the peatland as well as vegetation samples (see Thomas et al. (2023a) for more site details). Core samples were taken by alternately coring two small hummocks about 20 cm apart to a depth of 340 cm. Plant samples were taken within a five-meter radius of the coring site, and multiple samples

of each species were mixed in their respective sample bags to avoid an outsize effect of individual sample heterogeneity (Jansen et al., 2006).

Four *Sphagnum* moss species were identified, along with *Polytrichum strictum*. A few shrubs were found: *Calluna vulgaris*, *Empetrum nigrum*, *Oxycoccus palustris*, *Vaccinium myrtillus*, *Vaccinium uliginosum*, and *Vaccinium vitis-idaea*. Additionally, *Eriophorum vaginatum* was present. The peatland was surrounded by a spruce-dominated wooded area, but on the peat itself, there were a few smaller trees growing, including *Pinus sylvestris*, *Picea abies*, *Betula pendula*, and *Betula pubescens*.

### SAMPLE PREPARATION

The plant samples were kept cold with ice packs until they could be stored at -20°C. Prior to freeze-drying, the samples were separated into their constituent parts as well as possible. Separated into leaves, woody aboveground tissue (hereafter referred to as "stems"), and roots were *C. vulgaris*, *V. myrtillus*, *V. uliginosum*, *V. vitis-idaea*, *E. nigrum* (there was not enough root material to analyze for *E. nigrum*), *B. pendula*, and *B. pubescens*. Separated into needles, stems, and roots were *P. sylvestris* and *P. abies*. Separated into aboveground (non-woody) biomass and roots were *O. palustris* and *E. vaginatum*. The five moss species (*P. strictum*, *S. angustifolium*, *S. capillifolium*, *S. fuscum*, and *S. magellanicum*) were measured as whole plant samples. All samples were freeze-dried to a constant weight and then homogenized using a ball mill.

The subsampling procedure of the peat core is described in detail in Thomas et al. (2023a). Briefly, the core was split into 5 cm intervals, except for a few visibly distinct layers at 10–12 cm, 170–172 cm, 270–272 cm, 325–327 cm, 327–328 cm, and 337.5–340 cm. The peat samples were also freeze-dried to a constant weight and homogenized using a ball mill.

### ELEMENTAL ANALYSIS

Carbon and nitrogen concentrations (C, N) were measured using an Elemental Analyzer-Isotope Ratio Mass Spectrometer (EA-IRMS; Flash 2000 HT-Plus, linked by ConFlo IV to DELTA V Plus IRMS; Thermo Fisher Scientific). Stable C and N isotopes were also measured. Two replicates were analyzed for each sample. Measurement calibration was performed using caffeine (Merck, Germany) and a soil reference material from a Chernozem

(Harsum, Germany; see Black Carbon Reference Materials, <https://www.geo.uzh.ch/en/units/2b/Services/BCmaterial/Environmental-matrices.html>).

## BIOMARKER EXTRACTION AND ANALYSIS

The procedure followed for the biomarker extraction and analysis is described in full in Thomas et al. (2023a). Soxhlet extraction was performed on the milled plant samples following Wiesenberg & Gocke (2015). Dichloromethane (DCM): methanol (MeOH) (93:7, v/v) was used as the solvent, and each extraction ran for approximately 30 hours. The total lipid extracts were separated into three fractions: a neutral fraction containing *n*-alkanes and *n*-alkanols, a fraction containing *n*-fatty acids, and a final fraction containing polar and high molecular weight compounds. The neutral fraction was further separated into aliphatic, aromatic, and heterocompound fractions.

Internal standards of deuterated *n*-tetracosane (D<sub>50</sub>C<sub>24</sub>, Cambridge Isotope Laboratories, Inc.), deuterated *n*-octadecanol (D<sub>37</sub>C<sub>18</sub>, Cambridge Isotope Laboratories, Inc.), and deuterated *n*-eicosanoic acid (D<sub>39</sub>C<sub>20</sub>, Cambridge Isotope Laboratories, Inc.) were added to the *n*-alkane, *n*-alkanol, and *n*-fatty acid fractions, respectively. Before measurement, the *n*-fatty acid fraction was methylated using a boron trifluoride-methanol solution (CAS #373-57-9, Sigma-Aldrich), and the *n*-alkanol fraction was silylated using N,O-bis(trimethylsilyl)-acetamide (BSA) (CAS #10416-59-8, Sigma-Aldrich).

Quantification was performed using a GC (Agilent 7890B) equipped with a multimode inlet and a flame ionization detector (FID). Identification was performed on a GC (Agilent 6890N) equipped with a split-splitless injector in splitless mode coupled to a MS (Agilent 5973). Both instruments had a DB-5MS column (50 m x 0.2 mm x 0.33 μm) and 1.5 m deactivated pre-column and used helium as the carrier gas (1 ml min<sup>-1</sup>). The GC oven temperature for *n*-alkanes was held at 70°C for 4 min and increased to 320°C at a rate of 5°C min<sup>-1</sup> held for 50 min. For *n*-fatty acids and *n*-alkanols, the temperature was held at 50°C for 4 min, then increased to 150°C at a rate of 4°C min<sup>-1</sup>, and finally increased to 320°C at a rate of 3°C min<sup>-1</sup> held for 40 min. The GC-MS was operated in electron ionization mode at 70 eV and scanned from m/z 50–550. Individual compounds were identified by comparison of mass spectra with those of external standards and from the NIST and Wiley mass spectra library.

## DATA ANALYSIS

### BIOMARKER MEASUREMENTS

All biomarker measurements were calculated in units of microgram per gram dry weight. Several equations have been developed during past research to better evaluate biomarker concentrations and their indications. One such index measurement is the Carbon Preference Index (CPI); for *n*-alkanes, this measures the proportion of odd chain lengths to even chain lengths, and for *n*-alkanols and *n*-fatty acids, this measures the proportion of even chain lengths to odd chain lengths. A CPI greater than 1 indicates that the biomarkers are likely derived from a higher terrestrial plant; CPIs closer to or less than 1 are likely to be degraded organic matter or have a microbial source (Cranwell, 1981). The CPI formula we used for the *n*-alkanes is from Marzi et al., 1993:

$$CPI_{ALK} = \frac{(\sum_{i=n}^m C_{2i+1} + \sum_{i=n+1}^{m+1} C_{2i})}{2(\sum_{i=n+1}^{m+1} C_{2i})} \quad (1)$$

Where *n* = the starting chain length divided by 2 and *m* = the ending chain length divided by 2. We used *n*=10 and *m*=16 for the *n*-alkanes. For the *n*-alkanols and *n*-fatty acids, the formula was slightly adjusted:

$$CPI_{ALC/FA} = \frac{(\sum_{i=n}^m C_{2i} + \sum_{i=n+1}^{m+1} C_{2i})}{2(\sum_{i=n+1}^{m+1} C_{2i+1})} \quad (2)$$

We used *n* = 10 and *m*=14 for the *n*-alkanols and *n*=10 and *m*=16 for the *n*-fatty acids.

The Average Chain Length (ACL) is another index used to help interpret biomarker data. It is the average of the individual chain lengths (Poynter et al., 1989) and has previously been used to make a distinction between vegetation types and as an indicator for environmental conditions such as drought (e.g., Crausbay et al., 2014; Wüthrich et al., 2017). The formula for the *n*-alkanols and *n*-fatty acids was again slightly adjusted, and the same *n* and *m* values were used as for the CPI equations.

$$ACL_{ALK} = \frac{\sum_{i=n}^m (2i+1) * C_{2i+1}}{\sum_{i=n}^m C_{2i+1}} \quad (3)$$

$$ACL_{ALC/FA} = \frac{\sum_{i=n}^m (2i) * C_{2i}}{\sum_{i=n}^m C_{2i}} \quad (4)$$

$P_{aq}$  and  $P_{wax}$  are proxies developed to determine different sources of *n*-alkanes.  $P_{aq}$  was initially used to determine the proportion of aquatic macrophytes to terrestrial plant inputs in sediments (Ficken et al., 2000) and subsequently used in peatlands to infer past water levels, with higher values of  $P_{aq}$  implying a higher water table (e.g., Andersson et al., 2011; Zheng et al., 2007; Zhou et al., 2005).  $P_{wax}$  is used to determine the input of terrestrial plants (Zheng et al., 2007).

$$P_{aq} = \frac{C_{23}+C_{25}}{C_{23}+C_{25}+C_{29}+C_{31}} \quad (5)$$

$$P_{wax} = \frac{C_{27}+C_{29}+C_{31}}{C_{23}+C_{25}+C_{27}+C_{29}+C_{31}} \quad (6)$$

Other indicative ratios between biomarker chain lengths have been identified in previous studies, including for *n*-alkanes  $C_{23}/C_{25}$  (Bingham et al., 2010; McClymont et al., 2008),  $C_{23}/(C_{27}+C_{31})$  (Andersson et al., 2011),  $C_{23}/(C_{23}+C_{29})$ , and  $C_{25}/(C_{25}+C_{29})$  (Ronkainen et al., 2013), and *n*-alkanols  $C_{22}/C_{24}$ ,  $(C_{22}+C_{24})/(C_{26}+C_{28})$  (Zheng et al., 2011), and  $C_{24}/C_{28}$ , as well as for *n*-fatty acids  $C_{15}/(C_{15}+C_{16})$  (Zheng et al., 2007) and  $C_{24}/C_{28}$  (Thomas et al., 2023). We calculated all of these to identify which ones might be the most applicable in the Beerberg setting.

#### STATISTICAL ANALYSIS

Principal component analysis (PCA) was performed using the biomarker concentrations and the calculated ratios (eq. 1 to 6) to determine which linear combination of these could best separate the plant and peat core samples and which contributed the most variance. The PCAs were performed using the R packages "FactoMineR" (Husson et al., 2023) and "factoextra" (Kassambara & Mundt, 2020). The PCAs were used to describe the structure of the biomarker data from the Beerberg samples in addition to the univariate methods.

## VERHIB

The VERHIB model mentioned in the introduction is fully described in Jansen et al., 2010. It consists of a linear regression model describing the accumulation of plant-derived biomarkers over time in an archive; this forward model is inverted to estimate the plant assemblage that was most likely to have been present. Briefly, the forward model is based on the equation:

$$\begin{bmatrix} b_1(d, t) \\ \vdots \\ b_i(d, t) \end{bmatrix} = \begin{bmatrix} lf_1(d)lc_{1,1} & \cdots & lf_j(d)lc_{1,j} & rf_1(d)rc_{1,1} & \cdots & rf_j(d)rc_{1,j} \\ \vdots & \ddots & \vdots & \vdots & \ddots & \vdots \\ lf_1(d)lc_{i,1} & \cdots & lf_j(d)lc_{i,j} & rf_1(d)rc_{i,1} & \cdots & rf_j(d)rc_{i,j} \end{bmatrix} \begin{bmatrix} lm_1(t) \\ \vdots \\ lm_j(t) \\ rm_1(t) \\ \vdots \\ rm_j(t) \end{bmatrix}$$

in which  $b_i(d, t)$  is the mass of biomarker  $i$  accumulated at depth  $d$  during time  $t$ ,  $lc_{i,j}$  is the concentration of biomarker  $i$  in the leaf of plant  $j$ ,  $rc_{i,j}$  is the concentration of biomarker  $i$  in the root of plant  $j$ ,  $lf_j(d)$  is the fraction of leaf mass of plant  $j$  accumulating at depth  $d$ , and  $rf_j(d)$  is the same for root mass,  $lm_j(t)$  is the leaf mass of plant  $j$  during time  $t$  and  $rm_j(t)$  is the root mass of plant  $j$  during time  $t$ . The leaf to root mass ratio is a parameter that can be specified for each plant species based off of field data, literature, or estimation. Additionally, each plant's leaf and root biomass must be greater than or equal to zero as a constraint. It is also important to carefully consider which plant species to include in the database for the model as they should be those most likely to occur in the investigated location over the specified time period.

The inverse model is based on the matrix equation:

$$b = Ap$$

Where  $b$  is a vector of the biomarker composition in each depth layer,  $A$  is a matrix containing known constants, including those related to plant groupings and autocorrelation between depth layers, and  $p$  is a matrix of the parameters to be solved for. The equation is solved using a least-squares approach. Additionally, it is possible to specify two additional coefficients to increase the weight of the autocorrelation and the plant groupings to smooth the results.

We calculated the Pearson correlation coefficient between the predicted core biomarker composition ( $y$ ) and the actual values ( $x$ ) using the equation:

$$r = \frac{\sum(x - \bar{x})(y - \bar{y})}{\sqrt{\sum(x - \bar{x})^2 \sum(y - \bar{y})^2}}$$

The Pearson correlation coefficient was used to check for equifinality.

## RESULTS

### BIOMARKER COMPOSITION OF MODERN PLANTS

We report the results of the biomarker measurements from the modern plant samples for *n*-alkanes C<sub>21</sub>-C<sub>33</sub>, *n*-alkanols C<sub>20</sub>-C<sub>28</sub>, and *n*-fatty acids C<sub>20</sub>-C<sub>32</sub>. The total abundance of the three compound classes, the chain length of their most abundant homologues, and their respective CPI and ACL measurements, as well as the P<sub>aq</sub> and P<sub>wax</sub> values for the *n*-alkanes and the C%, N%, and delta C values, are shown in Table 1 for each plant species and part. The complete dataset of measurements is available at <https://doi.pangaea.de/10.1594/PANGAEA.961142> (Thomas et al., 2023b). Selected parameters are shown in the boxplots in Figure 1, grouped by plant functional type (Moss, Sedge, Shrubs, and Trees) and plant part (Moss, Leaves/non-woody Aboveground biomass, Needles, Stems, Roots).

The average C and N concentration and stable <sup>13</sup>C isotope values for the moss samples were 45.4%, 0.7%, and -28.9, respectively. For the shrub leaf and aboveground samples, the averages were 50.5%, 0.9%, and -29.7. The averages for the shrub stems were 49.2%, 0.5%, and -29.0. The averages for the shrub roots were 48.0%, 0.5%, -28.2. There was only one sedge species, *E. vaginatum*, and the values for its aboveground biomass were 46.6%, 1.1%, and -26.6. The values for the roots were 45.6%, 1.0%, and -25.8. The averages for the tree needles were 49.4%, 1.1%, and -28.2, and for the tree leaves were 48.8%, 1.3%, and -28.2. The tree stem averages were 50.3%, 0.8%, and -28.6; the tree root averages were 48.2%, 0.9%, and -27.3 (Table 1).

Across all species and plant parts, some general trends could be identified. Largely, the *n*-fatty acids were the compound class with the highest absolute concentration, usually greater than the *n*-alkane and *n*-alkanol absolute concentrations by an order of magnitude. Between the *n*-alkanes and *n*-alkanols, *n*-alkanes were typically more abundant in leaves/non-woody aboveground biomass. In contrast, *n*-alkanols were primarily the more abundant compound class in stem and root samples. Of the *n*-alkanes, C<sub>31</sub> was most often the most abundant homologue (C<sub>max</sub>) in 21 out of 35 samples, followed by C<sub>29</sub> in 8 samples. For *n*-alkanols, C<sub>28</sub> was the most frequent C<sub>max</sub> in 11 of 35 samples, closely followed by C<sub>24</sub> in 9 samples.

For *n*-fatty acids, C<sub>24</sub> was the most frequent C<sub>max</sub> in 14 of 35 samples, followed by C<sub>20</sub> and C<sub>28</sub>, both occurring as C<sub>max</sub> in 6 samples (Table 1).

The CPI<sub>ALK</sub> tended to be higher in aboveground biomass samples (excluding the coniferous needles) than in the other plant parts (Fig. 1). The ACL<sub>ALK</sub> also tended to be higher in aboveground biomass samples, though tree roots had a higher average than both deciduous tree leaves and coniferous needles (Fig. 1a). The highest average values for both C<sub>23</sub>/C<sub>25</sub> and C<sub>23</sub>/(C<sub>27</sub>+C<sub>31</sub>) were for the coniferous tree needles and the tree stems, followed by the moss samples. This also held for average P<sub>aq</sub> values, while the highest average P<sub>wax</sub> value was for shrub leaves, followed by tree roots and shrub stems and roots (Fig. 1a). The highest average values for both C<sub>23</sub>/(C<sub>23</sub>+C<sub>29</sub>) and C<sub>25</sub>/(C<sub>25</sub>+C<sub>29</sub>) were for the tree stems and the moss samples, followed by the coniferous needles. CPI<sub>ALC</sub> values were highest in tree stems, deciduous leaves, and coniferous needles, while ACL<sub>ALC</sub> values were highest in deciduous tree leaves and shrub leaves (Fig. 1b). The highest average values for the *n*-alkanol C<sub>22</sub>/C<sub>24</sub> ratio were in tree roots and stems while the lowest were in the moss samples and *E. vaginatum*. The highest values for the *n*-alkanol (C<sub>22</sub>+C<sub>24</sub>)/(C<sub>26</sub>+C<sub>28</sub>) ratio were for tree stems and coniferous needles. The highest average values for C<sub>24</sub>/C<sub>28</sub> were in the moss samples, followed by *E. vaginatum*, then coniferous needles (Fig. 1b). The CPI<sub>FA</sub> values were highest in tree roots, and stem roots had the highest ACL<sub>FA</sub> values (Fig. 1c). The highest average values for C<sub>15</sub>/(C<sub>15</sub>+C<sub>16</sub>) were in the moss samples. The highest average values for C<sub>24</sub>/C<sub>28</sub> are in the tree stems and roots, followed by the coniferous needles and moss samples (Fig. 1c).

PCAs were performed using the biomarker data: the absolute concentrations of the plant-derived chain lengths and the values calculated for the ratios described in the Methods section. First, all identified biomarkers and ratios were included, with PC1 explaining 25.1% of the variance and PC2 21.6% (Fig. 2a). The top six variables contributing to the first and second PCs were P<sub>aq</sub>, P<sub>wax</sub>, C<sub>25</sub> *n*-alkane, C<sub>26</sub> and C<sub>28</sub> *n*-alkanols, and the *n*-alkane ratio C<sub>23</sub>/(C<sub>23</sub>+C<sub>29</sub>). There are distinct clusters of leaves, moss, and roots, while the stem samples are spread out, likely due to the high P<sub>aq</sub> values of the tree stem samples. Separate PCAs were also performed for each biomarker group and their respective ratios. The *n*-alkane PCA identified a PC1 accounting for 41.4% of the variance and PC2 for 23.1%, with C<sub>25</sub> *n*-alkane,

$P_{wax}$ ,  $P_{aq}$ ,  $ACL_{ALK}$ ,  $C_{23}/(C_{23}+C_{29})$ , and  $C_{25}/(C_{25}+C_{29})$  as the top six contributors (Fig. 2b). While the leaves and moss were separated well by the first two axes, the roots cluster completely overlapped with that of the moss and the stem cluster completely overlapped that of the moss and half of the leaf cluster. In the PCA of *n*-alkanol concentrations and ratios, PC1 accounted for 32.7% and PC2 accounted for 30% of the variance with the top six contributors being  $C_{20}$ ,  $C_{22}$ ,  $C_{26}$ , and  $C_{28}$  *n*-alkanol,  $ACL_{ALC}$ , and the  $(C_{22}+C_{24})/(C_{26}+C_{28})$  ratio (Fig. 2c). The leaves and root clusters were separated, but the roots cluster overlapped with that of the moss and the stems cluster overlapped the other three. The PCA with *n*-fatty acids identified PC1 accounting for 38.4% of the variance and PC2 accounting for 27.7%, with the top six contributors being  $C_{20}$ ,  $C_{22}$ ,  $C_{24}$ , and  $C_{30}$  *n*-fatty acids,  $CPI_{FA}$ , and  $ACL_{FA}$  (Fig. 2d). The leaves and roots clusters were separated, but the moss cluster overlapped a small part of each with the stems cluster overlapping part of the leaf and moss clusters.

**Table 1. Elemental and biomarker composition of modern plants at Beerberg peatland.**

Species	PFT	Plant part	Elemental			<i>n</i> -Alkanes						<i>n</i> -Alkanols				<i>n</i> -Fatty acids			
			C	N	Delta C	C <sub>max</sub>	Total (ug/g)	CPI	ACL	P <sub>aq</sub>	P <sub>wax</sub>	C <sub>max</sub>	Total (ug/g)	CPI	ACL	C <sub>max</sub>	Total (ug/g)	CPI	ACL
<i>Calluna vulgaris</i>	Evergreen shrub	Leaves	51.9±0.1	0.75±0	-30.4±0.2	31	2056	14.9	31.3	0.02	0.98	28	163	10.4	25.3	32	2543	7.8	27.1
		Stem	47.9±0.2	0.33±0	-30.4±0	31	370	11.6	30.6	0.10	0.91	28	228	15.2	25.7	28	1453	8.0	26.5
		Roots	47.5±0.4	1.05±0	-28.7±0.1	33	813	12.7	31.7	0.03	0.97	28	243	10.0	25.2	24	699	1.5	24.2
<i>Empetrum nigrum</i>	Evergreen shrub	Leaves	53.0±0.6	0.66±0	-29.1±0	31	2408	34.1	30.8	0.00	1.00	26	181	7.2	25.8	28	377	8.0	27.4
		Stem	51.2±0.7	0.31±0	-28.6±0.1	29	1725	35.3	30.1	0.00	1.00	28	169	28.4	26.7	30	677	17.3	27.5
<i>Oxycoccus palustris</i>	Evergreen shrub	Aboveground	50.4±1.2	0.60±0	-31.1±0.1	29	275	13.0	29.3	0.02	0.98	26	120	11.9	25.3	24	715	6.0	25.9
		Roots	50.1±0.3	0.55±0.1	-29.9±0.1	29	25	8.9	29.0	0.11	0.91	24	201	10.3	25.0	24	682	5.9	24.5
<i>Vaccinium myrtillus</i>	Deciduous shrub	Leaves	48.8±0.7	1.41±0	-29.9±0	31	461	10.7	30.6	0.01	0.99	24	284	14.5	24.8	20	502	4.3	25.5
		Stem	48.9±0	0.72±0	-30.3±0	31	131	3.0	29.7	0.06	0.94	24	143	13.7	24.2	30	465	5.3	26.8
		Roots	47.1±0.7	0.22±0	-29.2±0.2	31	5	NA	29.7	0.15	0.88	28	64	35.8	27.2	26	587	3.5	25.2
<i>Vaccinium uliginosum</i>	Deciduous shrub	Leaves	48.4±0.7	1.14±0	-29.7±0.1	27	131	5.6	26.3	0.87	0.66	28	309	6.2	26.4	28	3363	8.6	25.5
		Stem	48.8±0	0.79±0	-28.1±0.1	27	21	7.8	27.5	0.54	0.71	28	75	11.7	25.1	20	436	6.1	23.9
		Roots	47.7±0	0.40±0	-26.9±0.2	31	7	16.5	28.9	0.35	0.74	26	20	6.4	25.3	20	222	3.3	22.7
<i>Vaccinium vitis-idaea</i>	Evergreen shrub	Leaves	50.7±1.0	1.05±0	-28.2±0.1	29	316	8.0	28.1	0.23	0.82	26	58	3.9	26.0	20	403	4.7	25.6
		Stem	49.0±0.4	0.36±0	-27.5±0	29	644	4.6	28.7	0.14	0.89	24	113	5.0	23.5	30	309	4.2	26.1
		Roots	47.4±0.6	0.25±0	-26.5±0	31	36	5.6	29.2	0.17	0.85	26	46	12.2	26.0	26	170	5.1	26.2
<i>Eriophorum vaginatum</i>	Sedge	Aboveground	46.6±0.4	1.08±0	-26.6±0.1	31	1540	33.1	31.3	0.01	0.99	26	108	4.4	25.5	24	296	3.2	24.5
		Roots	45.6±0.2	0.99±0	-25.8±0.1	31	69	14.1	29.7	0.13	0.88	24	94	9.0	25.3	24	307	5.0	24.2
<i>Pinus sylvestris</i>	Evergreen coniferous tree	Needles	49.9±0.7	2.30±0	-27.5±0.1	29	24	6.4	28.6	0.26	0.78	24	194	8.4	24.9	22	1024	9.7	23.2
		Stem	48.3±0.1	0.64±0	-27.6±0	31	5	4.5	29.3	0.17	0.85	22	195	89.9	22.5	22	2359	23.6	22.2
		Roots	48.3±0.4	0.87±0	-26.6±0.1	31	5	6.9	30.1	0.15	0.87	22	13	7.3	22.2	24	1037	17.2	22.8
<i>Picea abies</i>	Evergreen coniferous tree	Needles	49.6±1.2	0.50±0	-30.5±0	29	13	4.7	27.8	0.40	0.66	22	28	41.2	22.8	22	559	8.7	24.0
		Stem	51.4±0	0.45±0	-30.5±0.1	23	19	5.5	26.8	0.54	0.52	22	142	3.6	22.6	24	2966	23.9	22.8
		Roots	48.2±0.3	0.56±0	-26.5±0.1	29	111	33.5	30.1	0.01	1.00	22	23	0.9	23.2	20	382	13.2	22.2
<i>Betula pendula</i>	Deciduous tree	Leaves	50.9±0.3	1.08±0	-28.7±0	31	955	22.8	27.0	0.20	0.85	28	312	26.3	25.0	28	1172	5.1	26.3
		Stem	51.6±0.1	1.10±0	-26.8±0	27	494	42.6	26.2	0.85	0.58	22	480	43.4	24.8	28	800	11.1	25.6
		Roots	48.3±0.4	0.91±0	-26.9±0	31	16	11.3	30.4	0.03	0.97	26	5	NA	24.1	20	115	1.2	22.3
<i>Betula pubescens</i>	Deciduous tree	Leaves	47.9±0.6	2.01±0.1	-30.4±0.1	31	1255	12.5	29.3	0.16	0.88	28	218	31.6	27.0	28	1356	4.4	26.1
		Stem	50.0±1.2	1.03±0	-29.5±0.1	25	499	32.6	26.5	0.76	0.48	28	535	35.3	25.6	26	1566	7.4	24.5
		Roots	48.2±0.9	1.20±0	-29.1±0.1	31	35	14.4	29.0	0.32	0.75	22	62	15.6	23.7	24	464	4.2	23.6
<i>Polytrichum strictum</i>	Moss		45.3±0.4	0.74±0	-28.7±0	31	46	6.4	30.0	0.13	0.89	28	23	5.5	25.9	24	433	5.2	24.6

<i>Sphagnum angustifolium</i>	Moss		46.4±0.2	0.78±0	-30.2±0.4	31	955	13.1	31.1	0.04	0.96	24	190	11.7	25.3	24	1201	5.4	26.4
<i>Sphagnum magellanicum</i>	Moss		43.8±1.0	0.77±0	-28.5±0.1	31	92	12.2	30.2	0.25	0.77	24	70	9.4	25.1	24	264	5.9	24.3
<i>Sphagnum capillifolium</i>	Moss		48.3±4.4	0.81±0.1	-29.1±0	31	95	5.6	27.7	0.44	0.62	24	124	9.5	25.1	24	380	4.2	24.9
<i>Sphagnum fuscum</i>	Moss		43.4±0	0.38±0	-27.9±0.1	31	200	15.5	29.7	0.36	0.7	26	137	12.6	25.2	24	236	6.3	25.5

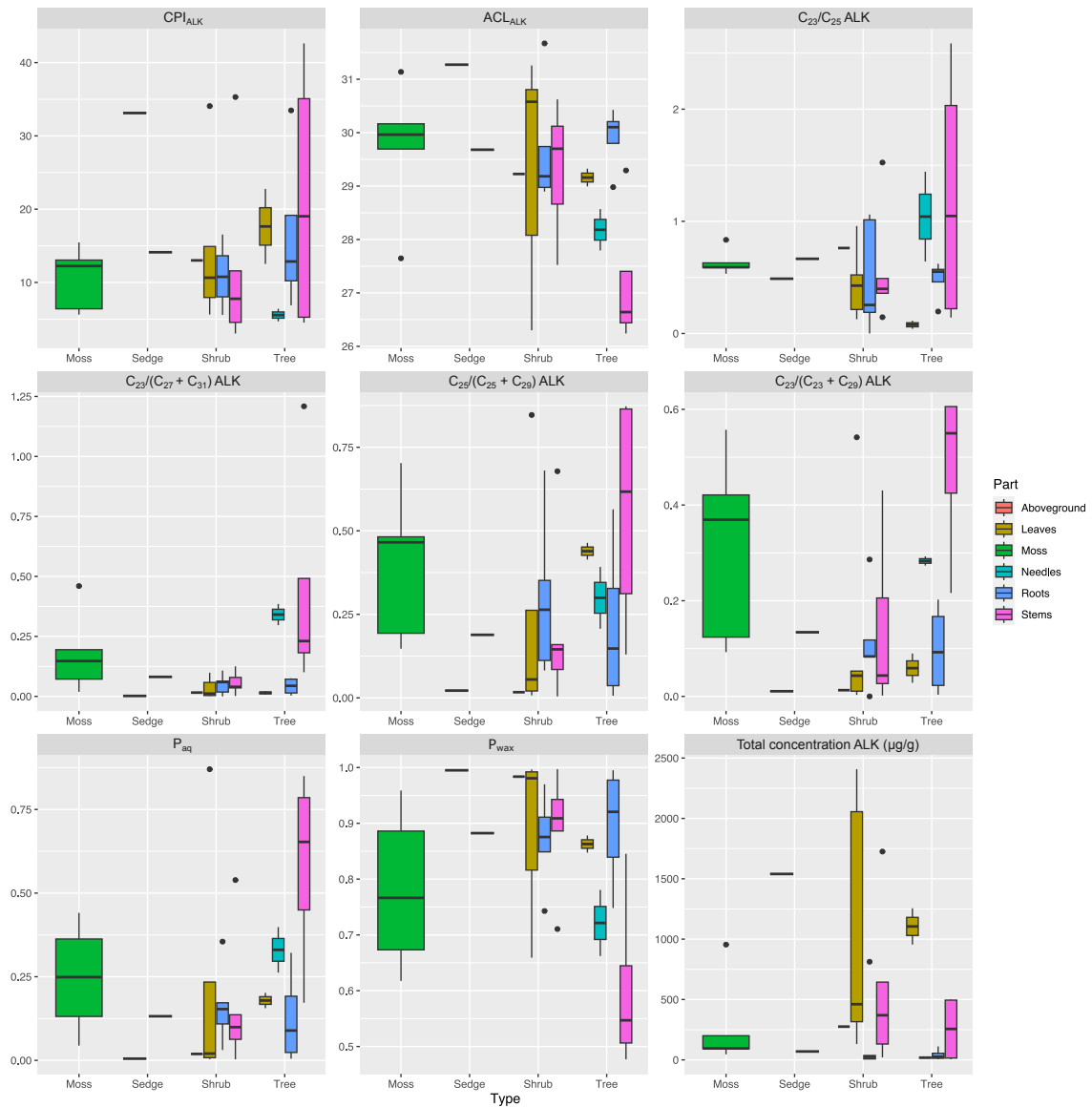


**Figure 1a: Boxplots of *n*-alkane variables in modern plant parts (CPI, ACL,  $C_{23}/C_{25}$ ,  $C_{23}/(C_{27}+C_{31})$ ,  $C_{25}/(C_{25}+C_{29})$ ,  $C_{23}/(C_{23}+C_{29})$ ,  $P_{aq}$ ,  $P_{wax}$ , and total concentration). Plant/part: moss-whole plant (n=5), sedge-aboveground biomass (n=1), sedge-roots (n=1), shrub-aboveground biomass (n=1), shrub-leaves (n=5), shrub-roots (n=5), shrub-stems (n=5), tree-leaves (n=2), tree-needles (n=2), tree-roots (n=4), tree-stems (n=4).**

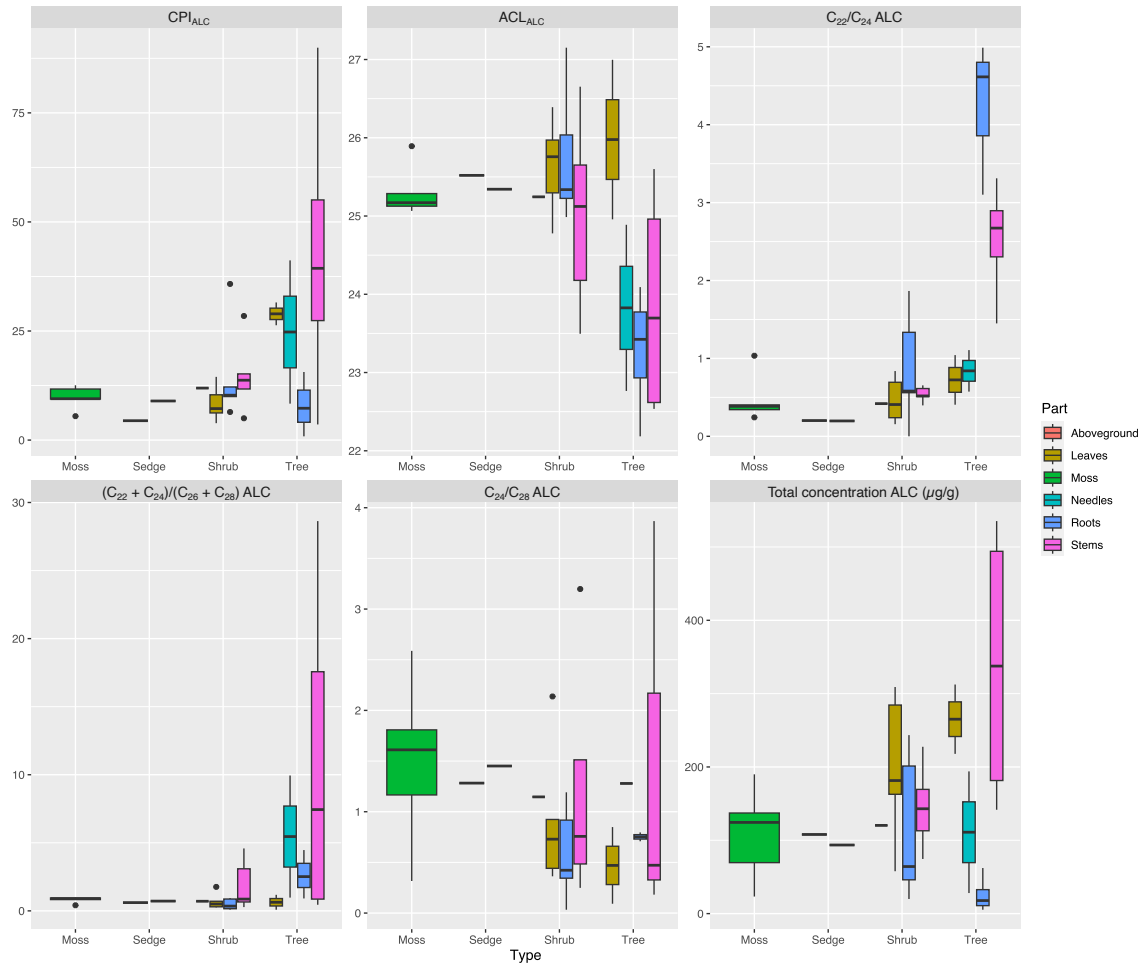


**Figure 1b: Boxplots of *n*-alkanol variables in modern plant parts (CPI, ACL, C<sub>22</sub>/C<sub>24</sub>, (C<sub>22</sub>+C<sub>24</sub>)/(C<sub>26</sub>+C<sub>28</sub>), C<sub>24</sub>/C<sub>28</sub>, and total concentration). Plant/part: moss-whole plant (n=5), sedge-aboveground biomass (n=1), sedge-roots (n=1), shrub-aboveground biomass (n=1), shrub-leaves (n=5), shrub-roots (n=5), shrub-stems (n=5), tree-leaves (n=2), tree-needles (n=2), tree-roots (n=4), tree-stems (n=4).**

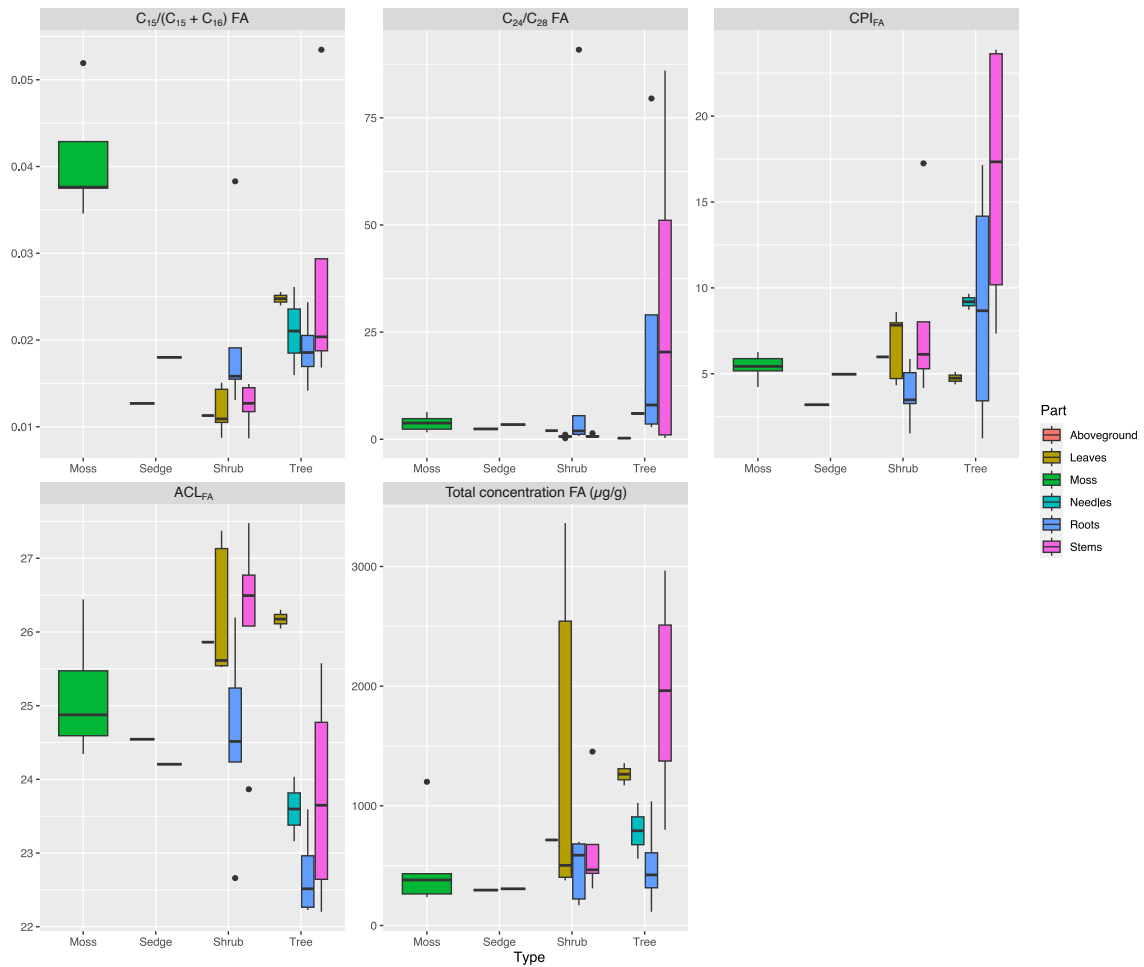


**Figure 1c: Boxplots of  $n$ -fatty acid variables in modern plant parts ( $C_{15}/(C_{15}+C_{16})$ ,  $C_{24}/C_{28}$ , CPI, ACL, and total concentration). Plant/part: moss-whole plant (n=5), sedge-aboveground biomass (n=1), sedge-roots (n=1), shrub-aboveground biomass (n=1), shrub-leaves (n=5), shrub-roots (n=5), shrub-stems (n=5), tree-leaves (n=2), tree-needles (n=2), tree-roots (n=4), tree-stems (n=4).**

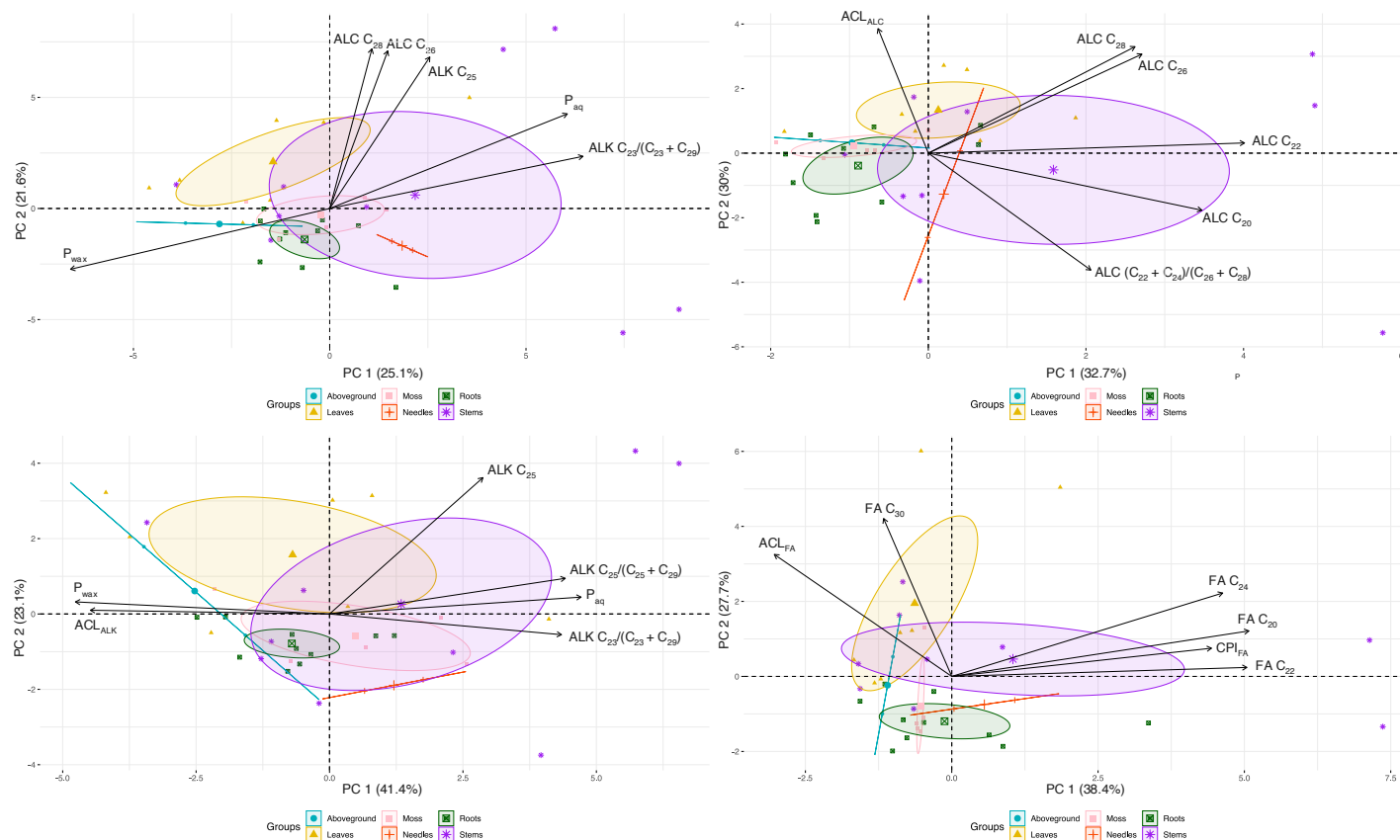


**Figure 2:** (a) PCA of plant samples using all plant-derived biomarker absolute concentrations, odd  $C_{21}$ - $C_{33}$   $n$ -alkanes, even  $C_{20}$ - $C_{28}$   $n$ -alkanols, and even  $C_{20}$ - $C_{32}$   $n$ -fatty acids, and the ACL and CPI for all of the compound groups, and the other ratios listed in the Methods section. The ellipses and lines represent a 95% confidence interval for each plant part group. (b) PCA of plant samples using the odd  $C_{21}$ - $C_{33}$   $n$ -alkanes, the ACL and CPI, and the other  $n$ -alkane ratios listed in the Methods section. The ellipses and lines represent a 95% confidence

interval for each plant part group. (c) PCA of plant samples using the even  $C_{20}$ - $C_{28}$   $n$ -alkanols, the ACL and CPI, and the other ratios listed in the Methods section. The ellipses and lines represent a 95% confidence interval for each plant part group. (d) PCA of plant samples using the even  $C_{20}$ - $C_{32}$   $n$ -fatty acids, and the ACL and CPI. The ellipses and lines represent a 95% confidence interval for each plant part group.

## PCAS OF BEERBERG CORE DATA

The *n*-alkane, *n*-alkanol, and *n*-fatty acid concentrations measured in a core from Beerberg peatland have been previously reported in Thomas et al. (2023a,b). The same sequence of PCAs was performed to examine the data from the peat core. The PCA including all ratios and biomarker concentrations identified PC1 as explaining 51.6% of the variance and PC2 as explaining 12.8% (Fig. 3a). The top six variables contributing to the first and second PCs were C<sub>29</sub> and C<sub>31</sub> *n*-alkanes, C<sub>22</sub> and C<sub>28</sub> *n*-alkanols, P<sub>wax</sub>, and the C<sub>25</sub>/(C<sub>25</sub>+ C<sub>29</sub>)ratio. The *n*-alkane PCA identified a PC1 accounting for 59.8% of the variance and PC2 for 23%, with the C<sub>25</sub>/(C<sub>25</sub>+ C<sub>29</sub>) ratio, P<sub>wax</sub>, P<sub>aq</sub>, ACL<sub>ALK</sub>, and C<sub>29</sub> and C<sub>31</sub> *n*-alkanes as the top six contributors (Fig. 3b). In the PCA of *n*-alkanol concentrations and ratios, PC1 accounted for 55.1% and PC2 accounted for 28.3% of the variance with the top six contributors being C<sub>22</sub>, C<sub>24</sub>, and C<sub>28</sub> *n*-alkanol, ACL<sub>ALC</sub>, the C<sub>22</sub>/C<sub>24</sub> ratio, and the (C<sub>22</sub>+C<sub>24</sub>)/(C<sub>26</sub>+C<sub>28</sub>) ratio (Fig. 3c). The PCA with *n*-fatty acids identified PC1 accounting for 60.3% of the variance and PC2 accounting for 17.7%, with the top six contributors being C<sub>22</sub>, C<sub>24</sub>, C<sub>26</sub>, C<sub>28</sub>, C<sub>30</sub>, and C<sub>32</sub> *n*-fatty acids (Fig. 3d).

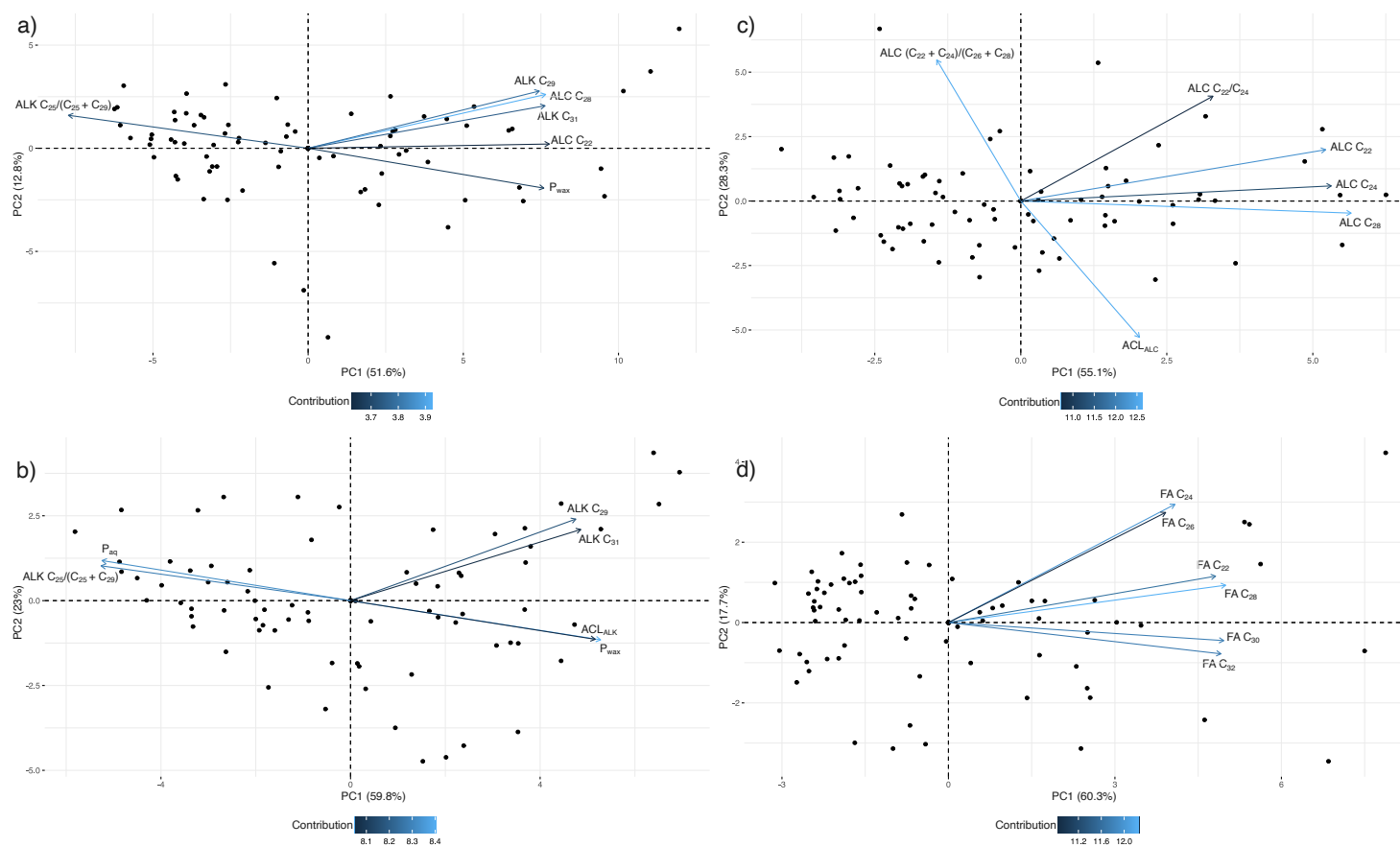


**Figure 3:** a) PCA of core samples using all plant-derived biomarker absolute concentrations, odd  $C_{21}$ - $C_{33}$   $n$ -alkanes, even  $C_{20}$ - $C_{28}$   $n$ -alkanols, and even  $C_{20}$ - $C_{32}$   $n$ -fatty acids, and the ACL and CPI for all of the compound groups, and the other ratios listed in the Methods section. (b) PCA of core samples using the odd  $C_{21}$ - $C_{33}$   $n$ -alkanes, the ACL and CPI, and the other  $n$ -alkane ratios listed in the Methods section. (c) PCA of core samples using the even  $C_{20}$ - $C_{28}$   $n$ -alkanols, the ACL and CPI, and the other ratios listed in

the Methods section. (d) PCA of core samples using the even  $C_{20}$ - $C_{32}$   $n$ -fatty acids, and the ACL and CPI.

## Modeling

### MATLAB MODEL

We used the original MATLAB version of the VERHIB model to run various scenarios and answer the following:

- a) Does adding *n*-fatty acid data help to create a more accurate and unique solution?
- b) Does adding root data help to create a more accurate and unique solution?

We compared the results to the macrofossil analysis included in Thomas et al. (2023b), as macrofossils are more representative of in situ vegetation than pollen analysis (Birks and Birks, 2000; Parnucci et al., 2015)

For the first group of scenarios (see Table 2 and Figs. 4 and 5), we included all of the chain lengths, not only plant-derived, and we did not include the root biomarker data. The two regularization parameters were kept at 0.1, and the maximum iterations were set at 2000. The plants were grouped as followed: Group 1: *S. angustifolium*, *S. magellanicum*, *S. capillifolium*, *S. fuscum*, Group 2: *C. vulgaris*, *V. uliginosum*, *V. myrtillus*, *V. vitis-idaea*, *O. palustris*, *E. nigrum*, Group 3: *E. vaginatum*, Group 4: *P. strictum*, Group 5: *P. sylvestris*, Group 6: *P. abies*, and Group 7: *B. pendula* and *B. pubescens*. Run #1 included all three compound classes, Run #2 included *n*-alkanes and *n*-alkanols, Run #3 included only *n*-alkanes, and Run #4 included *n*-alkanes and *n*-fatty acids. In this group of scenarios, Run #1 had a Pearson correlation coefficient between the predicted and actual core measurement values of 0.7476, Run #2 of 0.9963, Run #3 of 0.9995, and Run #4 of 0.7367. When comparing the VERHIB reconstructions to the plant macrofossil analysis, if *n*-fatty acid data was excluded (Figs. 4b and 4c), the contribution of tree species was overestimated, particularly *P. abies*, as was the contribution of *S. capillifolium* and *S. magellanicum*. However, all of the runs underestimated the presence of *E. vaginatum*, especially in the lowest part of the core. Figure 5 shows that the highest residuals typically occurred in the lowest depth layers.

In the second group of scenarios (Table 2 and Figs. 6 and 7), we again included all of the chain lengths and the root biomarker data, with a leaf:root mass ratio of 5:1. The two regularization parameters were kept at 0.1, and the maximum iterations were set at 2000.

The plant groupings remained the same. Run #5 included all three compound classes, Run #6 included *n*-alkanes and *n*-alkanols, Run #7 included only *n*-alkanes, and Run #8 included *n*-alkanes and *n*-fatty acids. Run #5 had a Pearson correlation coefficient between the predicted and actual core measurement values of 0.7436, Run #6 of 0.9962, Run #7 of 0.9952, and Run #8 of 0.9255. The results for this group of scenarios were similar to the first in that *E. vaginatum* was underestimated in all of the scenarios. In Fig. 6a, the contribution of *P. sylvestris* is overestimated in the lowest depth layers. In Fig. 6b, the estimated contribution of the plant species did not vary throughout the core as expected, and the contribution of *Sphagnum* mosses was underestimated. Figure 7 shows again that the highest residuals typically occurred in the lowest depth layers.

For the third group of scenarios (see Table 2 and Figs. 8 and 9), we included only plant-derived chain lengths and did not include the root biomarker data. The parameters, maximum iterations, and plant groupings were the same as the previous runs. Run #9 included all three compound classes, Run #10 included *n*-alkanes and *n*-alkanols, Run #11 included only *n*-alkanes, and Run #12 included *n*-alkanes and *n*-fatty acids. In this group of scenarios, Run #9 had a Pearson correlation coefficient between the predicted and actual core measurement values of 0.9783, Run #10 of 0.9972, Run #11 of 0.9995, and Run #12 of 0.9759. Again, all of the runs underestimated the proportion of *E. vaginatum*. In Figs. 8a and 8d, the contribution of *S. magellanicum* is overestimated. In Figs. 8b and 8c, the contribution of *P. sylvestris* and *P. abies* is overestimated. Figure 9 shows that the highest residuals typically occurred in the lowest depth layers, though there are also high residuals in the upper depth layers for Run #11 and throughout the core for Run #10.

For the last group of scenarios (see Table 2 and Figs. 10 and 11), we included only the plant-derived chain lengths and the root biomarker data, with a leaf:root mass ratio of 5:1. The parameters, maximum iterations, and plant groupings were kept the same as the previous runs. Run #13 included all three compound classes, Run #14 included *n*-alkanes and *n*-alcohols, Run #15 included only *n*-alkanes, and Run #16 included *n*-alkanes and *n*-fatty acids. In this group of scenarios, Run #13 had a Pearson correlation coefficient between the predicted and actual core measurement values of 0.7476, Run #14 of 0.9963, Run #15 of 0.9995, and Run #16 of 0.7367. The primary difference between the reconstructions of this group (Fig. 10) with the last group (plant-derived, no root data) (Fig. 8) is that the estimated

contribution of *P. strictum* increased in all the scenarios. The residual patterns also stayed very similar (Fig. 11).

**Table 2. Details of VERHIB runs and Pearson correlation coefficients.**

Run #	Compounds included	Leaf:root ratio	Reg (depth)	Reg (group)	Max iterations	Pearson coefficient (soil chem values)
1	ALK: C <sub>19</sub> -C <sub>33</sub> , ALC: C <sub>15</sub> -C <sub>28</sub> , FA: C <sub>14</sub> -C <sub>32</sub>	1:0	0.1	0.1	2000	0.7476
2	ALK: C <sub>19</sub> -C <sub>33</sub> , ALC: C <sub>15</sub> -C <sub>28</sub> ,	1:0	0.1	0.1	2000	0.9963
3	ALK: C <sub>19</sub> -C <sub>33</sub> ,	1:0	0.1	0.1	2000	0.9995
4	ALK: C <sub>19</sub> -C <sub>33</sub> , FA: C <sub>14</sub> -C <sub>32</sub>	1:0	0.1	0.1	2000	0.7367
5	ALK: C <sub>19</sub> -C <sub>33</sub> , ALC: C <sub>15</sub> -C <sub>28</sub> , FA: C <sub>14</sub> -C <sub>32</sub>	5:1	0.1	0.1	2000	0.7436
6	ALK: C <sub>19</sub> -C <sub>33</sub> , ALC: C <sub>15</sub> -C <sub>28</sub> ,	5:1	0.1	0.1	2000	0.9962
7	ALK: C <sub>19</sub> -C <sub>33</sub> ,	5:1	0.1	0.1	2000	0.9952
8	ALK: C <sub>19</sub> -C <sub>33</sub> , FA: C <sub>14</sub> -C <sub>32</sub>	5:1	0.1	0.1	2000	0.9255
9	Plant-derived: ALK, ALC, FA	1:0	0.1	0.1	2000	0.9783
10	Plant-derived; ALK, ALC	1:0	0.1	0.1	2000	0.9972
11	Plant-derived; ALK	1:0	0.1	0.1	2000	0.9995
12	Plant-derived; ALK, FA	1:0	0.1	0.1	2000	0.9759
13	Plant-derived: ALK, ALC, FA	5:1	0.1	0.1	2000	0.9681
14	Plant-derived; ALK, ALC	5:1	0.1	0.1	2000	0.9971
15	Plant-derived; ALK	5:1	0.1	0.1	2000	0.9937
16	Plant-derived; ALK, FA	5:1	0.1	0.1	2000	0.9755

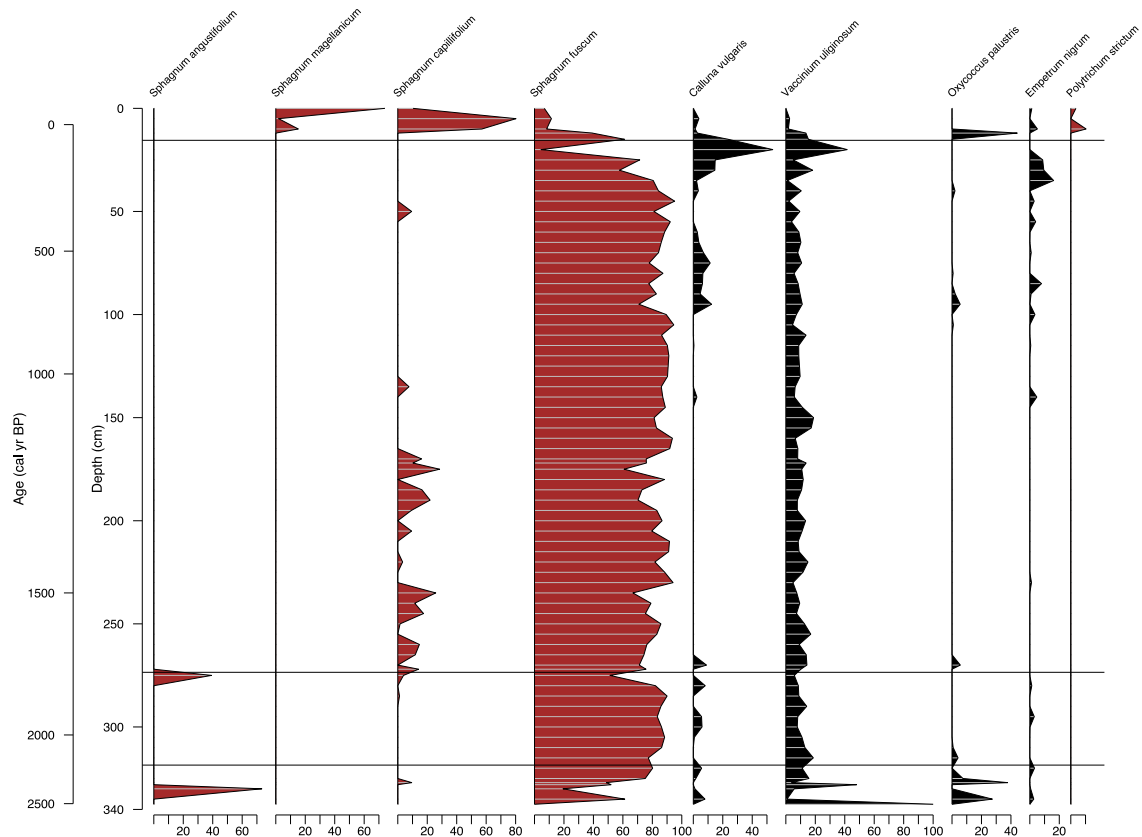


**Figure 4(a): VERHIB reconstruction for Run #1, showing calculated percentages of vegetation biomass input. Run #1 includes only leaf measurements and all chain length measurements for *n*-alkanes, *n*-alkanols, and *n*-fatty acids. The brown graphs are moss species, and the black graphs are shrub species. The phases identified in the Beerberg plant macrofossil analysis (Thomas et al., 2023b) are marked.**

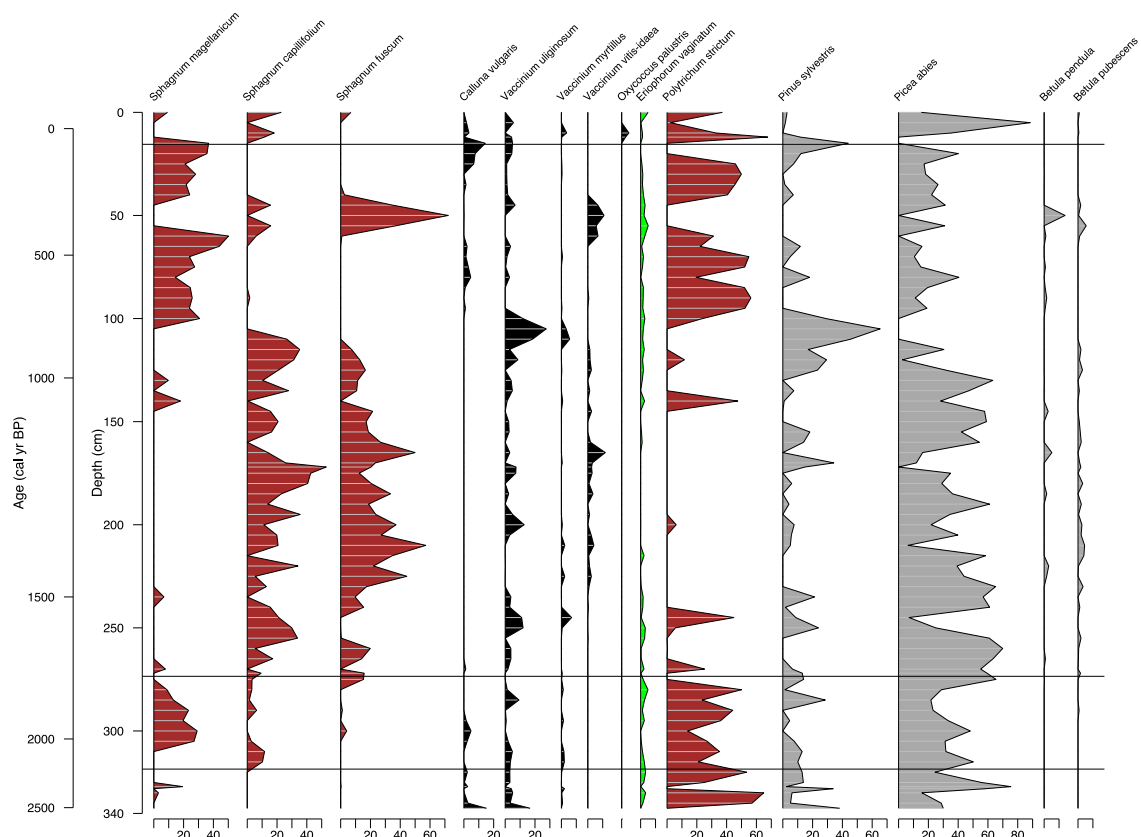


**Figure 4(b): VERHIB reconstruction for Run #2, showing calculated percentages of vegetation biomass input. Run #2 includes only leaf measurements and all chain length measurements for *n*-alkanes and *n*-alkanols. Brown graphs are moss species; black graphs are shrub species; green graph is *E. vaginatum*; and grey graphs are tree species. The phases identified in the Beerberg plant macrofossil analysis (Thomas et al., 2023b) are marked.**

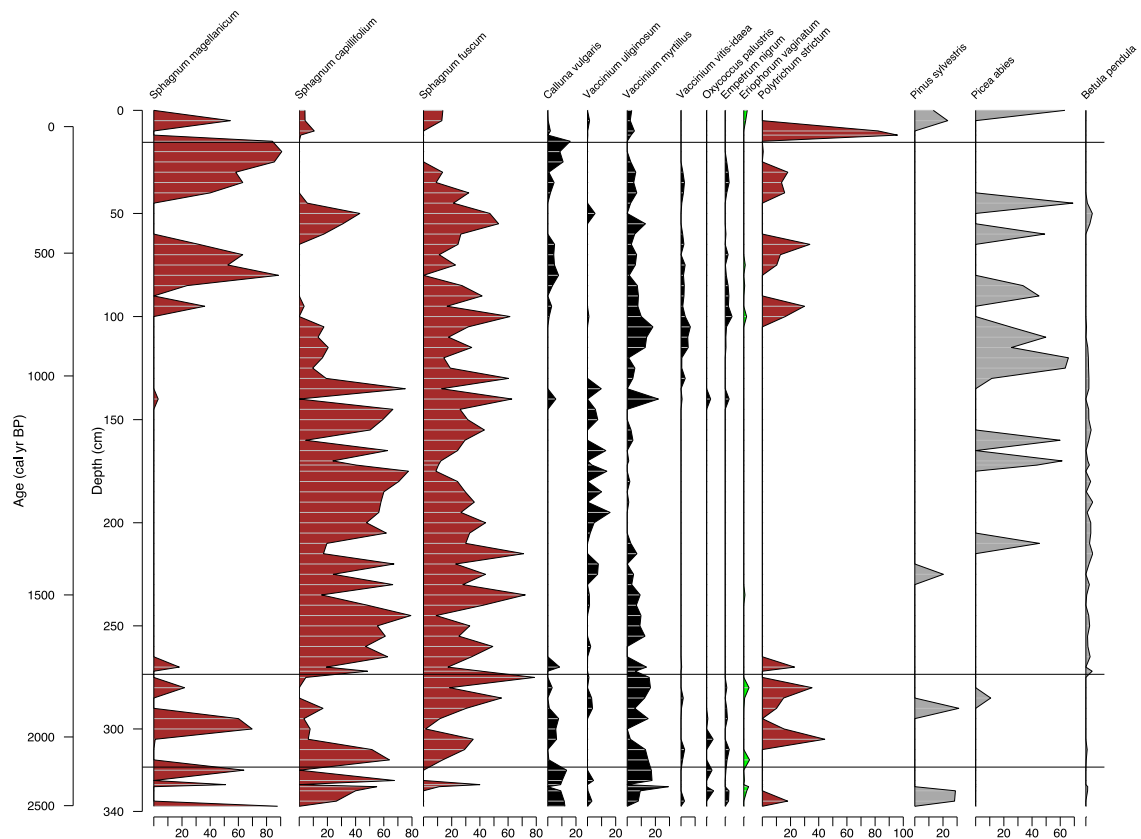


**Figure 4(c) VERHIB reconstruction for Run #3, showing calculated percentages of vegetation biomass input. Run #3 includes only leaf measurements and all chain length measurements for *n*-alkanes. Brown graphs are moss species; black graphs are shrub species; green graph is *E. vaginatum*; and grey graphs are tree species. The phases identified in the Beerberg plant macrofossil analysis (Thomas et al., 2023b) are marked.**

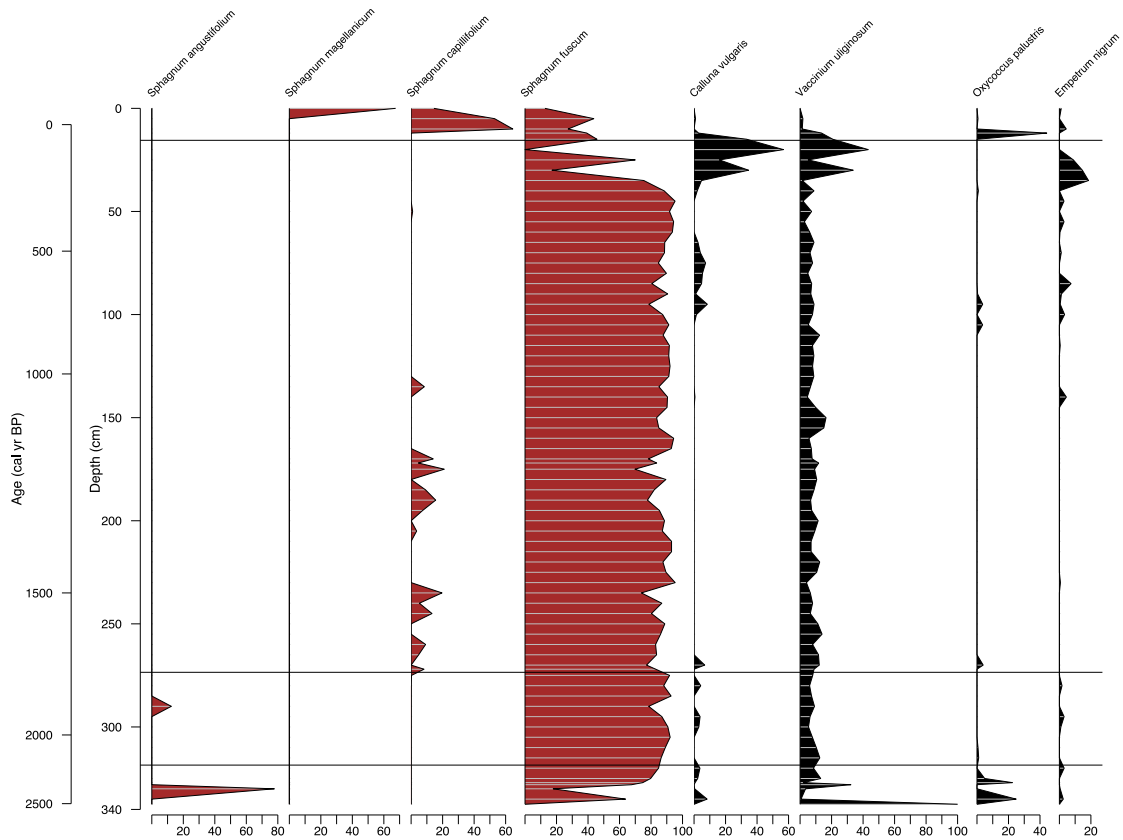


**Figure 4(d) VERHIB reconstruction for Run #4, showing calculated percentages of vegetation biomass input. Run #4 includes only leaf measurements and all chain length measurements for *n*-alkanes and *n*-fatty acids. Brown graphs are moss species, and black graphs are shrub species. The phases identified in the Beerberg plant macrofossil analysis (Thomas et al., 2023b) are marked.**



**Figure 5: Core measurement residuals versus depth for Run #1(a), Run #2 (b), Run #3 (c), and Run #4 (d), showing compounds with the highest residual values.**

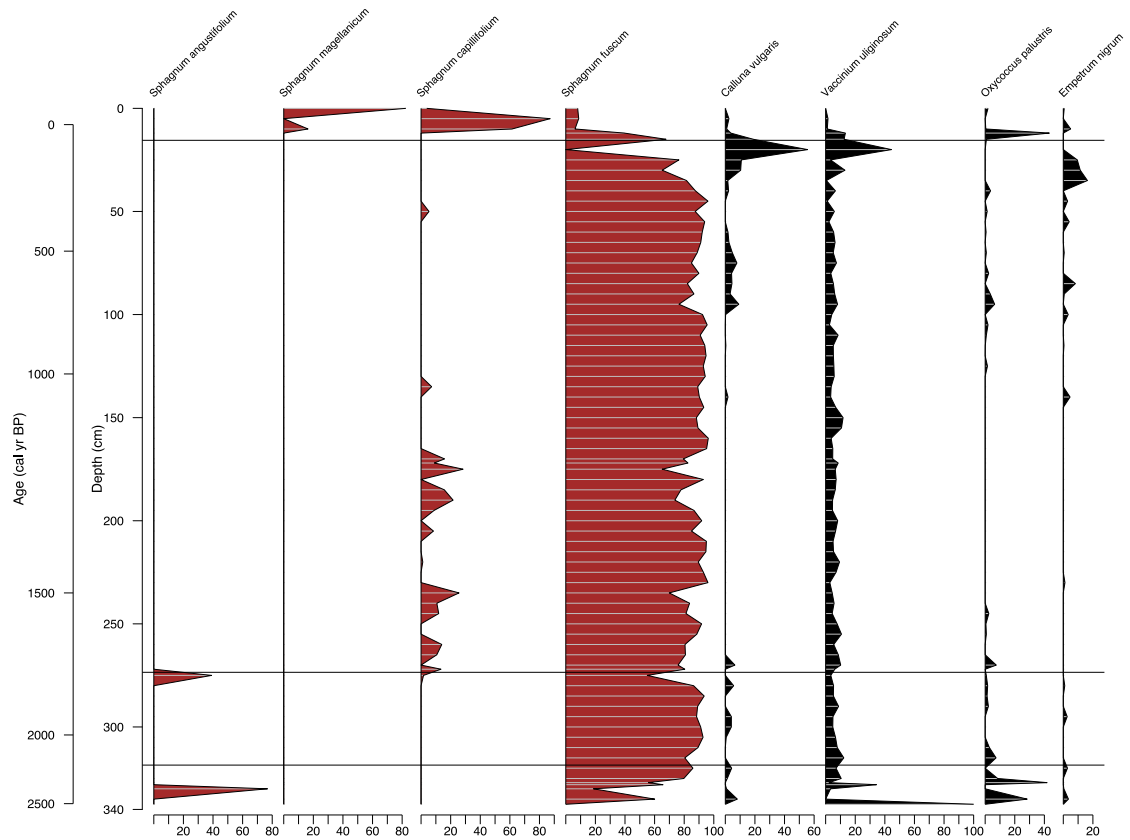


**Figure 6 (a) VERHIB reconstruction for Run #5, showing calculated percentages of vegetation biomass input. Run #5 includes leaf and root measurements (ratio leaf:root is 5:1) and all chain length measurements for *n*-alkanes, *n*-alkanols, and *n*-fatty acids. Brown graphs are moss species, and black graphs are shrub species. The phases identified in the Beerberg plant macrofossil analysis (Thomas et al., 2023b) are marked.**

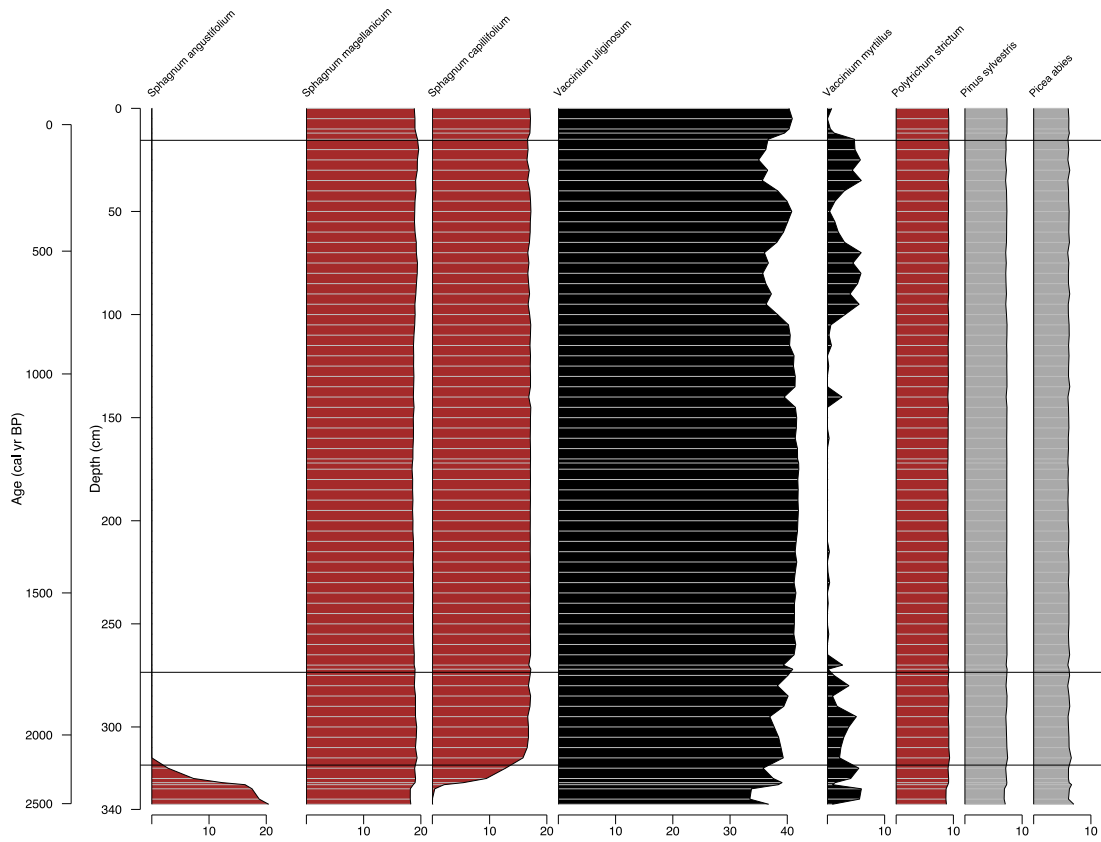


**Figure 6 (b) VERHIB reconstruction for Run #6, showing calculated percentages of vegetation biomass input. Run #5 includes leaf and root measurements (ratio leaf:root is 5:1) and all chain length measurements for *n*-alkanes and *n*-alkanols. Brown graphs are moss species, black graphs are shrub species, and grey graphs are tree species. The phases identified in the Beerberg plant macrofossil analysis (Thomas et al., 2023b) are marked.**

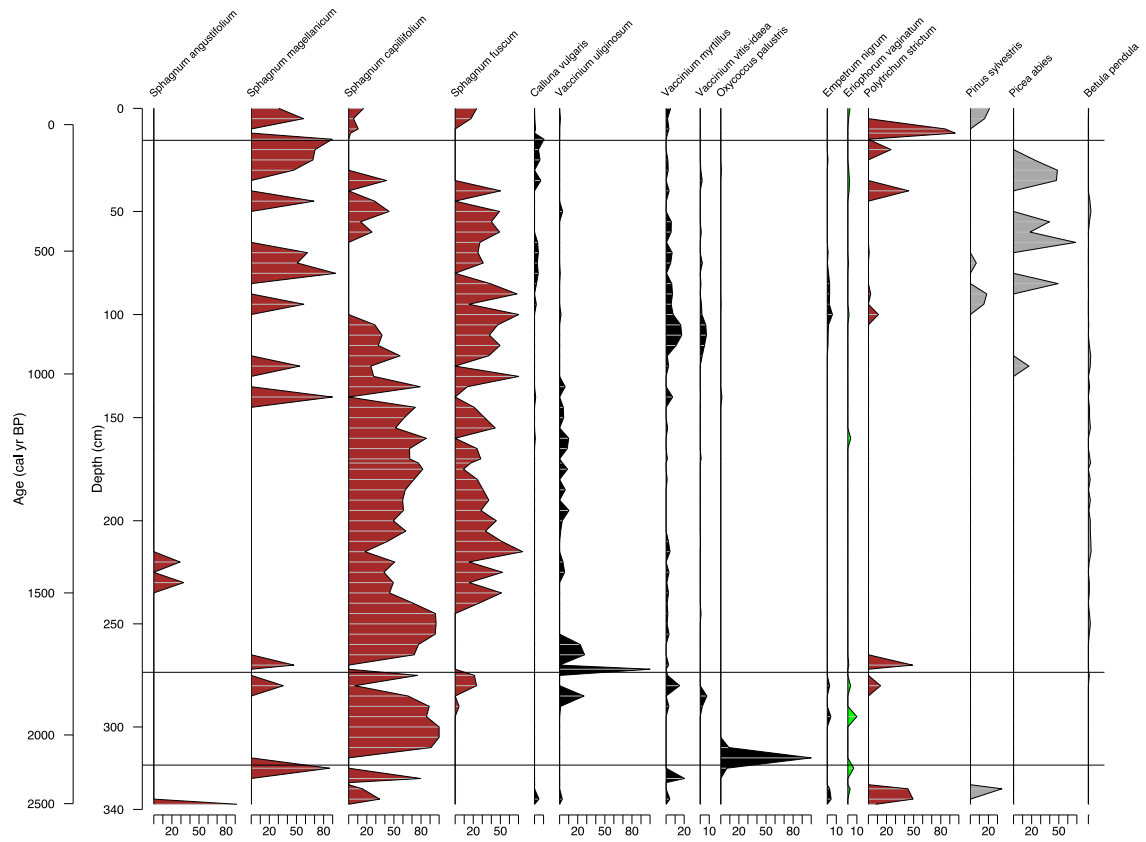


**Figure 6 (c) VERHIB reconstruction for Run #7, showing calculated percentages of vegetation biomass input. Run #7 includes leaf and root measurements (ratio leaf:root is 5:1) and all chain length measurements for *n*-alkanes. The brown graphs are moss species, the black graphs are shrub species, the green graph is *E. vaginatum*, and the grey graphs are tree species. The phases identified in the Beerberg plant macrofossil analysis (Thomas et al., 2023b) are marked.**

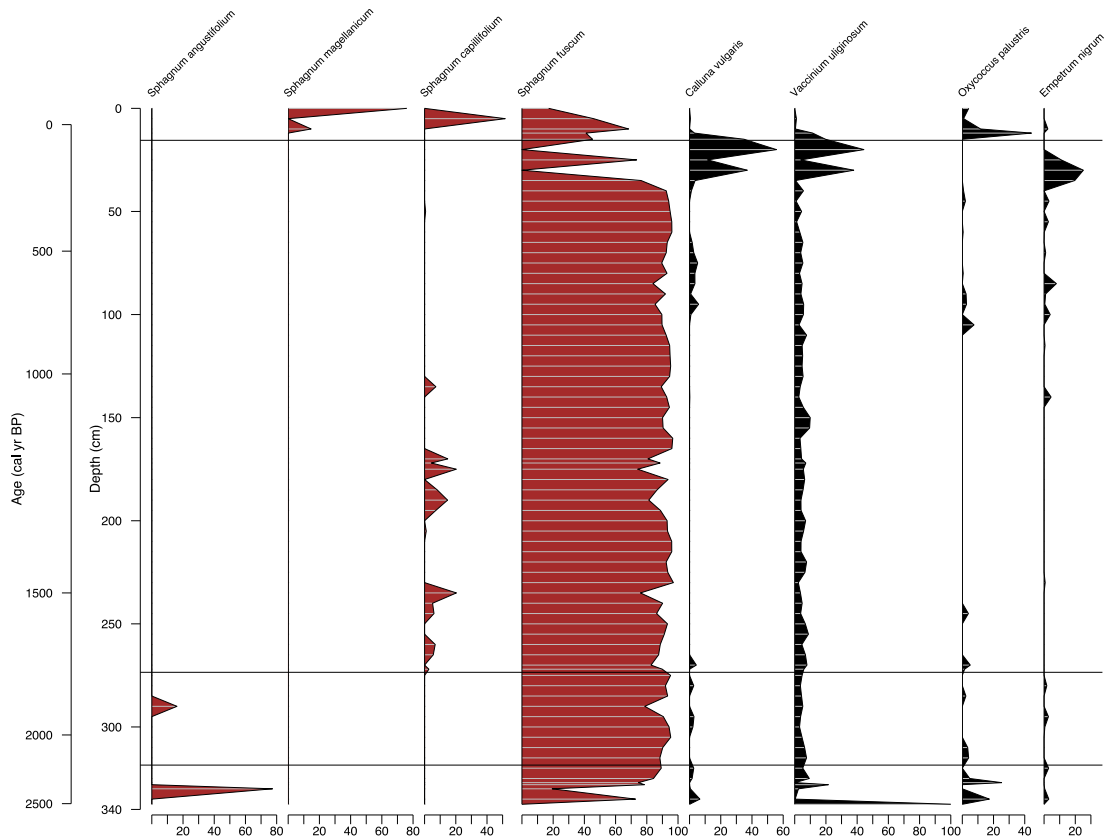


**Figure 6 (d) VERHIB reconstruction for Run #8, showing calculated percentages of vegetation biomass input. Run #8 includes leaf and root measurements (ratio leaf:root is 5:1) and all chain length measurements for *n*-alkanes and *n*-fatty acids. The brown graphs are moss species, and the black graphs are shrub species. The phases identified in the Beerberg plant macrofossil analysis (Thomas et al., 2023b) marked.**

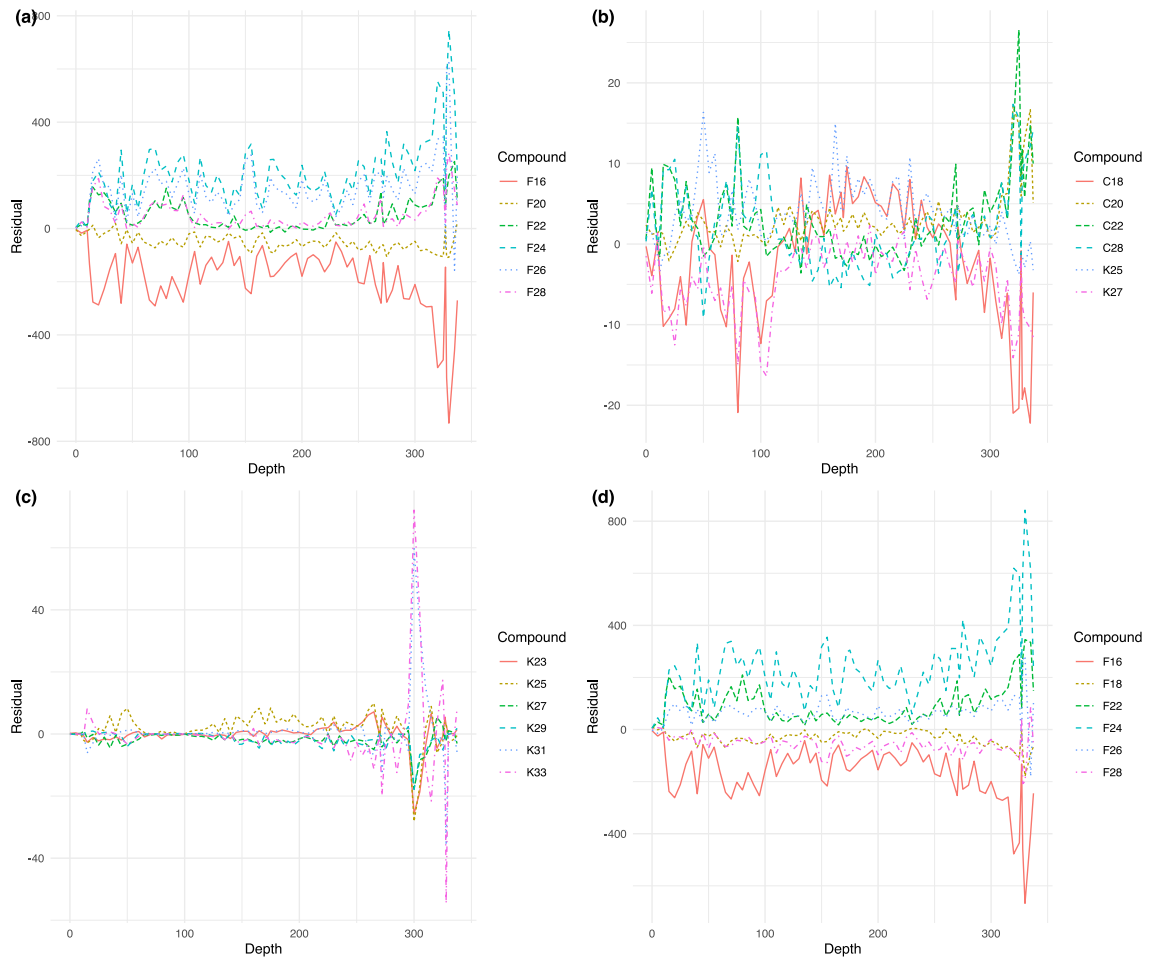


**Figure 7: Core measurement residuals versus depth for Run #5 (a), Run #6 (b), Run #7 (c), and Run #8 (d), showing compounds with the highest residual values.**

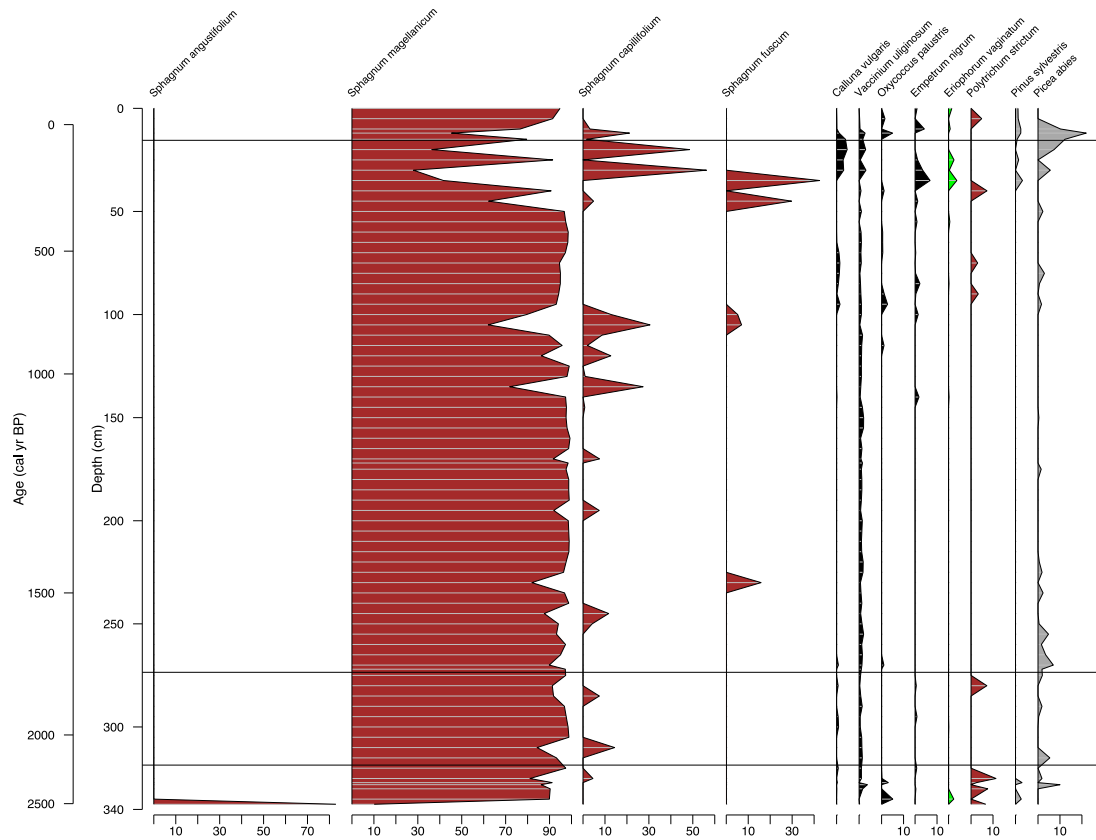


**Figure 8 (a) VERHIB reconstruction for Run #9, showing calculated percentages of vegetation biomass input. Run #9 includes only leaf measurements and only plant-derived chain length measurements for *n*-alkanes, *n*-alkanols, and *n*-fatty acids. Brown graphs are moss species; black graphs are shrub species; green graph is *E. vaginatum*; and grey graphs are tree species. The phases identified in the Beerberg plant macrofossil analysis (Thomas et al., 2023b) are marked.**

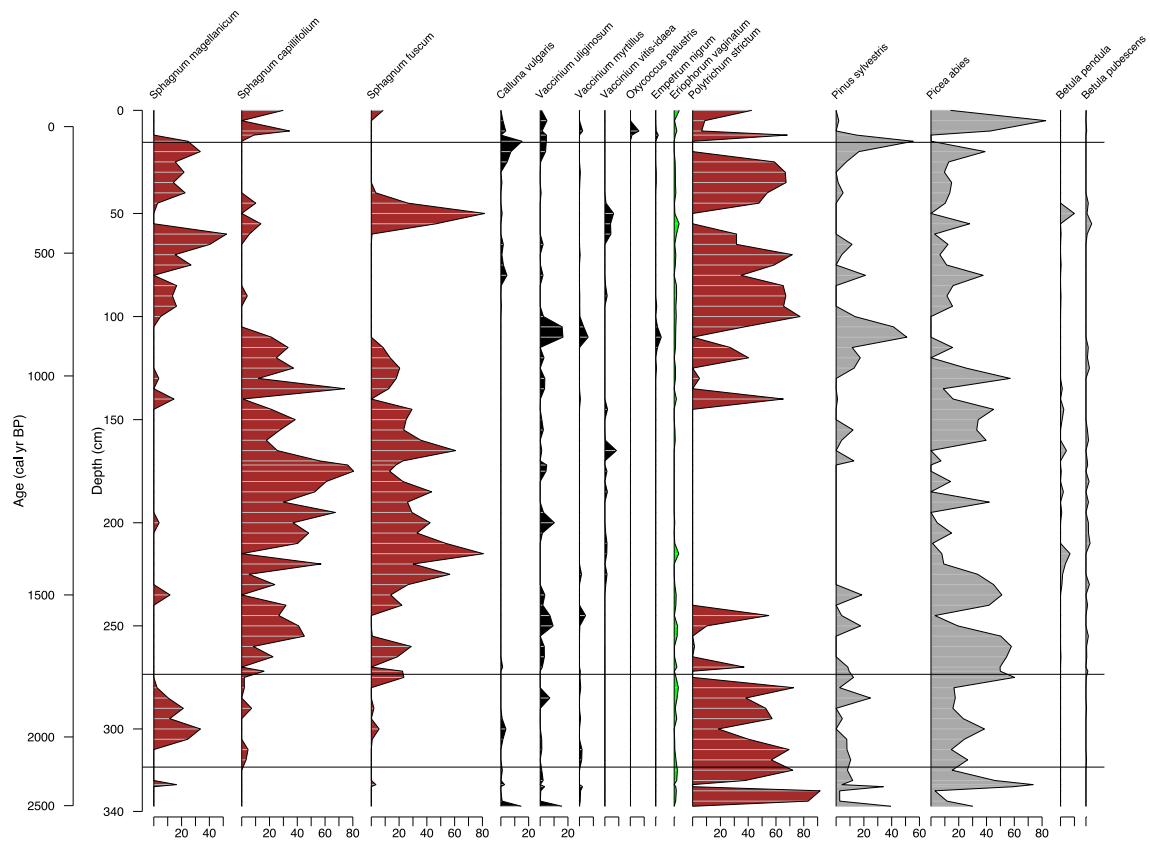


**Figure 8 (b) VERHIB reconstruction for Run #10, showing calculated percentages of vegetation biomass input. Run #10 includes only leaf measurements and only plant-derived chain length measurements for *n*-alkanes and *n*-alkanols. Brown graphs are moss species; black graphs are shrub species; green graph is *E. vaginatum*; and grey graphs are tree species. The phases identified in the Beerberg plant macrofossil analysis (Thomas et al., 2023b) are marked.**

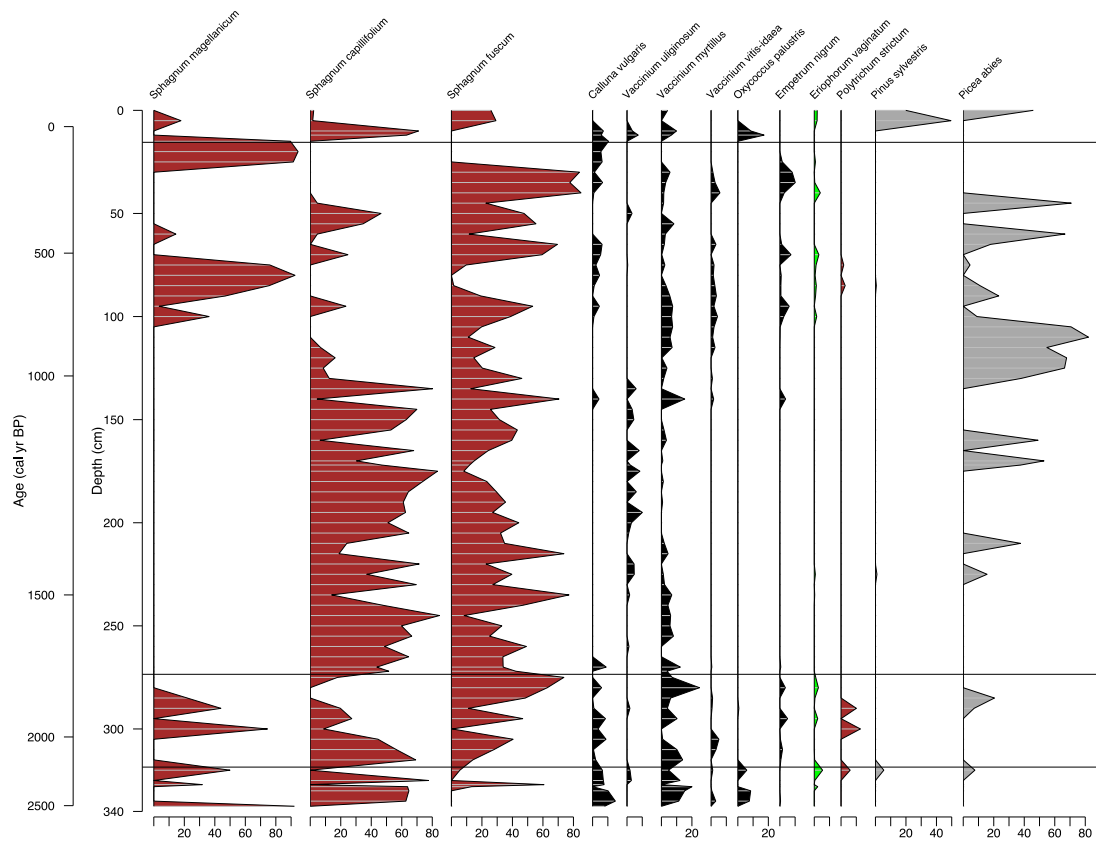


**Figure 8 (c) VERHIB reconstruction for Run #11, showing calculated percentages of vegetation biomass input. Run #11 includes only leaf measurements) and only plant-derived chain length measurements for *n*-alkanes. Brown graphs are moss species; black graphs are shrub species; green graph is *E. vaginatum*; and grey graphs are tree species. The phases identified in the Beerberg plant macrofossil analysis (Thomas et al., 2023b) are marked.**

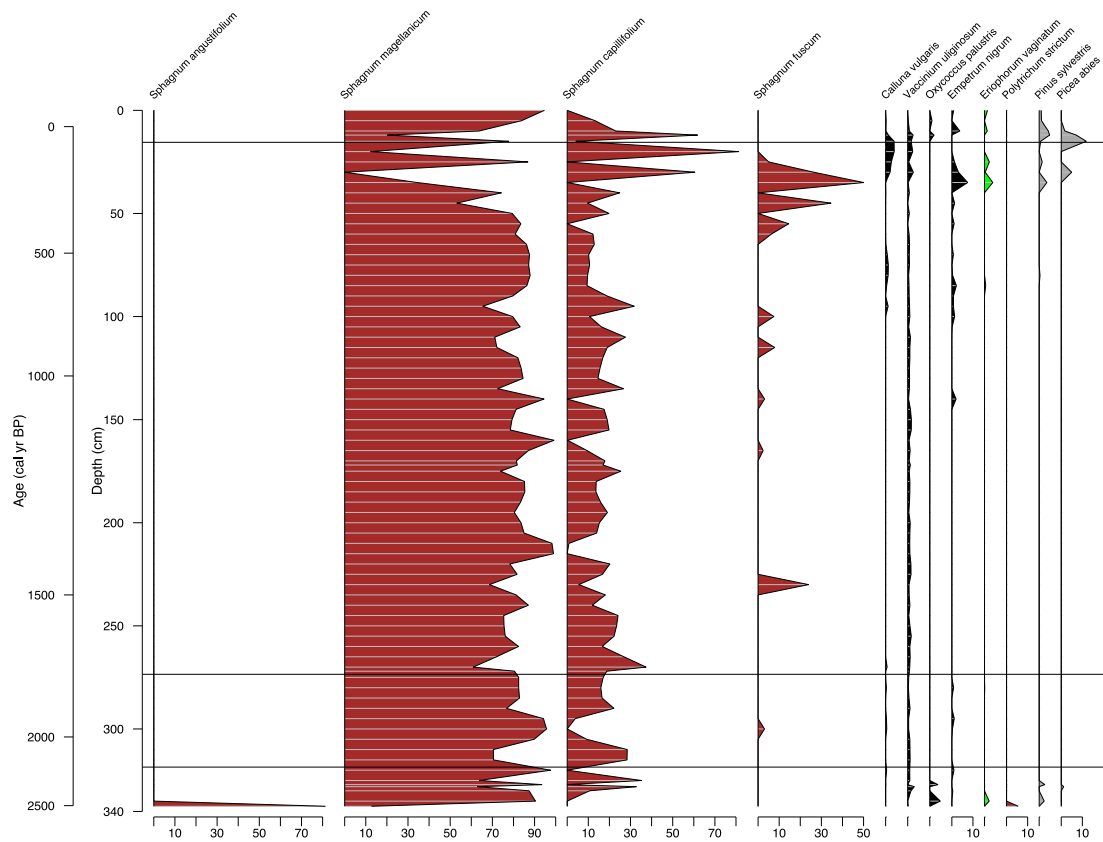


**Figure 8 (d) VERHIB reconstruction for Run #12, showing calculated percentages of vegetation biomass input. Run #12 includes only leaf measurements) and only plant-derived chain length measurements for *n*-alkanes and *n*-fatty acids. Brown graphs are moss species; black graphs are shrub species; green graph is *E. vaginatum*; and grey graphs are tree species. The phases identified in the Beerberg plant macrofossil analysis (Thomas et al., 2023b) are marked.**



**Figure 9: Core measurement residuals versus depth for Run #9(a), Run #10 (b), Run #11 (c), and Run #12 (d), showing compounds with the highest residual values.**

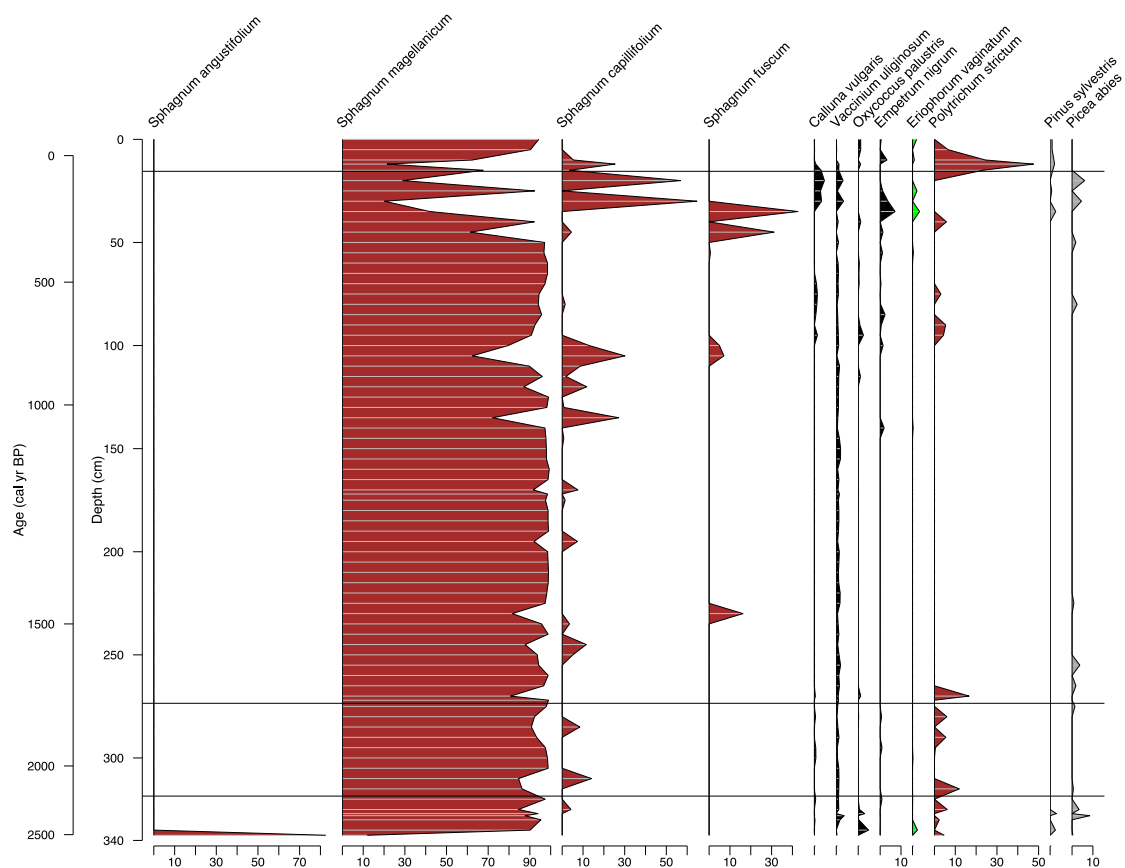


**Figure 10 (a) VERHIB reconstruction for Run #13, showing calculated percentages of vegetation biomass input. Run #13 includes leaf and root measurements (ratio leaf:root is 5:1) and only plant-derived chain length measurements for *n*-alkanes, *n*-alkanols, and *n*-fatty acids. Brown graphs are moss species; black graphs are shrub species; green graph is *E. vaginatum*; and grey graphs are tree species. The phases identified in the Beerberg plant macrofossil analysis (Thomas et al., 2023b) are marked.**

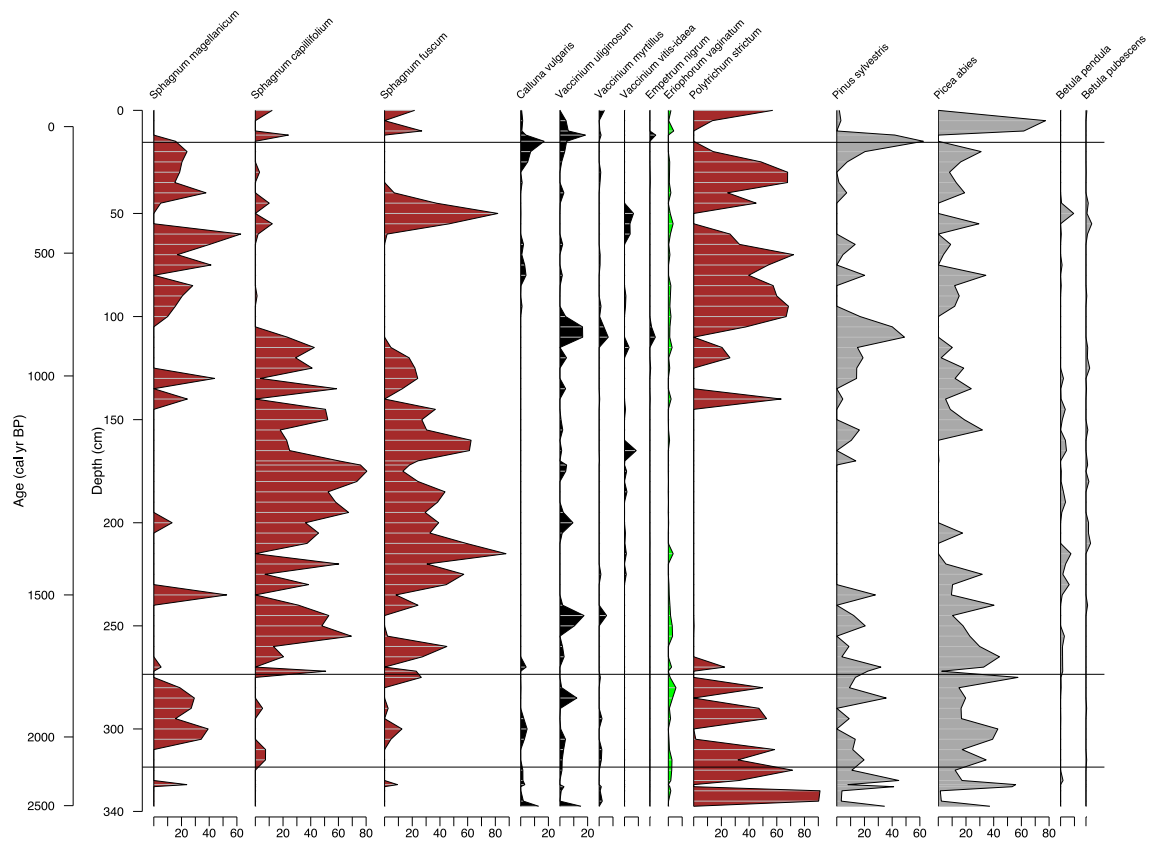


**Figure 10 (b) VERHIB reconstruction for Run #14, showing calculated percentages of vegetation biomass input. Run #14 includes leaf and root measurements (ratio leaf:root is 5:1) and only plant-derived chain length measurements for *n*-alkanes and *n*-alkanols. The brown graphs are moss species; the black graphs are shrub species; the green graph is *E. vaginatum*; and the grey graphs are tree species. The phases identified in the Beerberg plant macrofossil analysis (Thomas et al., 2023b) are marked.**

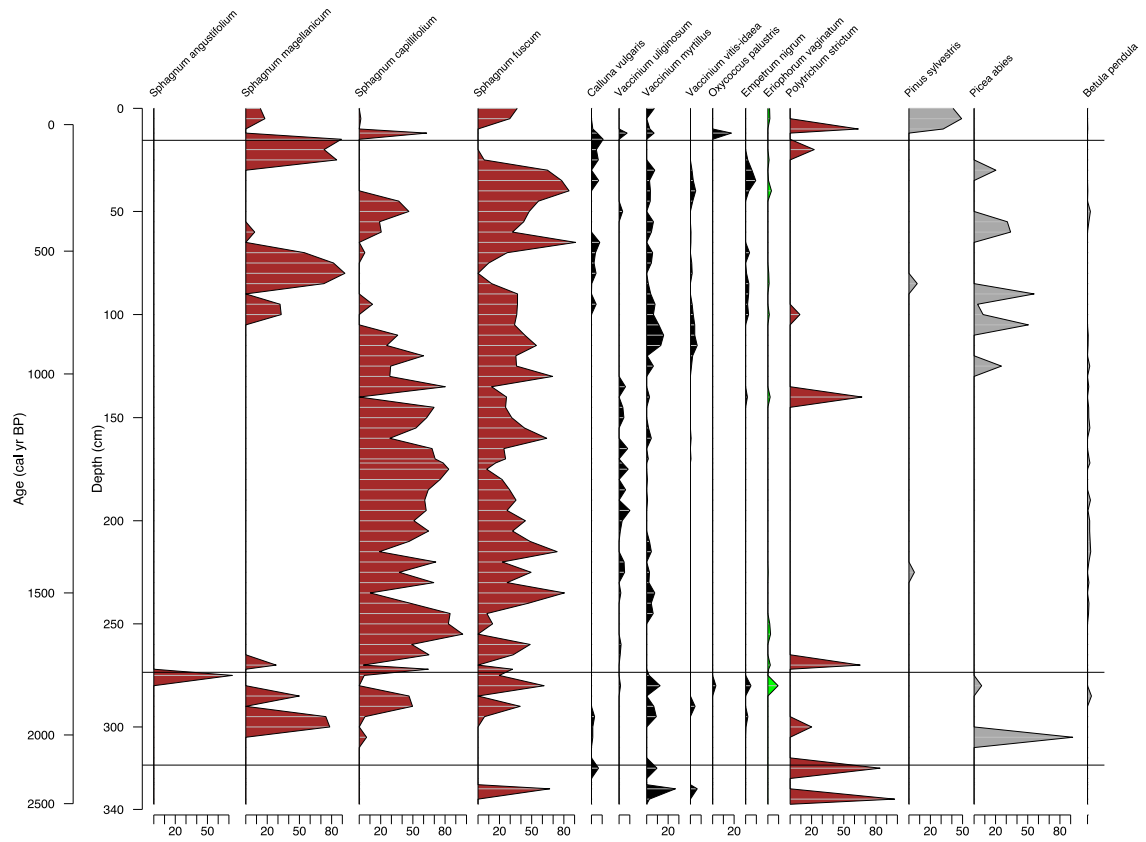


**Figure 10 (c) VERHIB reconstruction for Run #15, showing calculated percentages of vegetation biomass input. Run #15 includes leaf and root measurements (ratio leaf:root is 5:1) and only plant-derived chain length measurements for *n*-alkanes. The brown graphs are moss species, the black graphs are shrub species, the green graph is *E. vaginatum*, and the grey graphs are tree species. The phases identified in the Beerberg plant macrofossil analysis (Thomas et al., 2023b) are marked.**

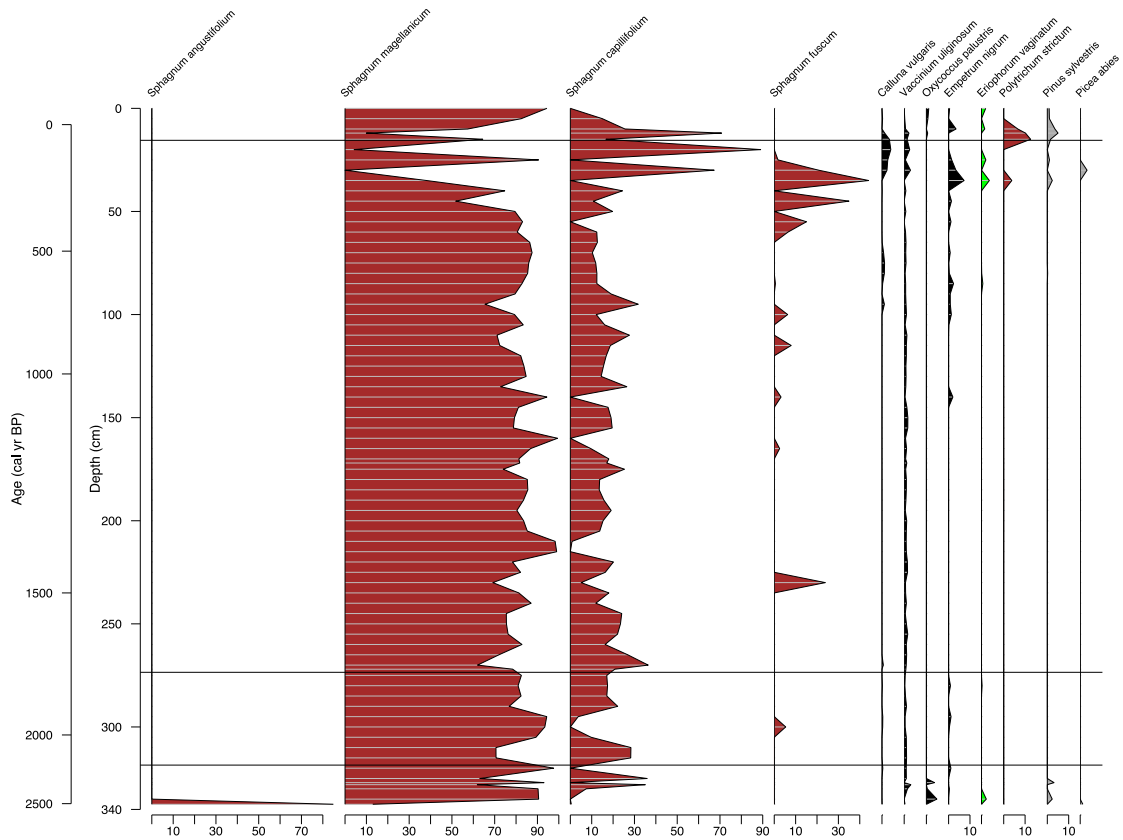


**Figure 10 (d) VERHIB reconstruction for Run #16, showing calculated percentages of vegetation biomass input. Run #16 includes leaf and root measurements (ratio leaf:root is 5:1) and only plant-derived chain length measurements for *n*-alkanes and *n*-fatty acids. The brown graphs are moss species, the black graphs are shrub species, the green graph is *E. vaginatum*, and the grey graphs are tree species. The phases identified in the Beerberg plant macrofossil analysis (Thomas et al., 2023b) are marked.**

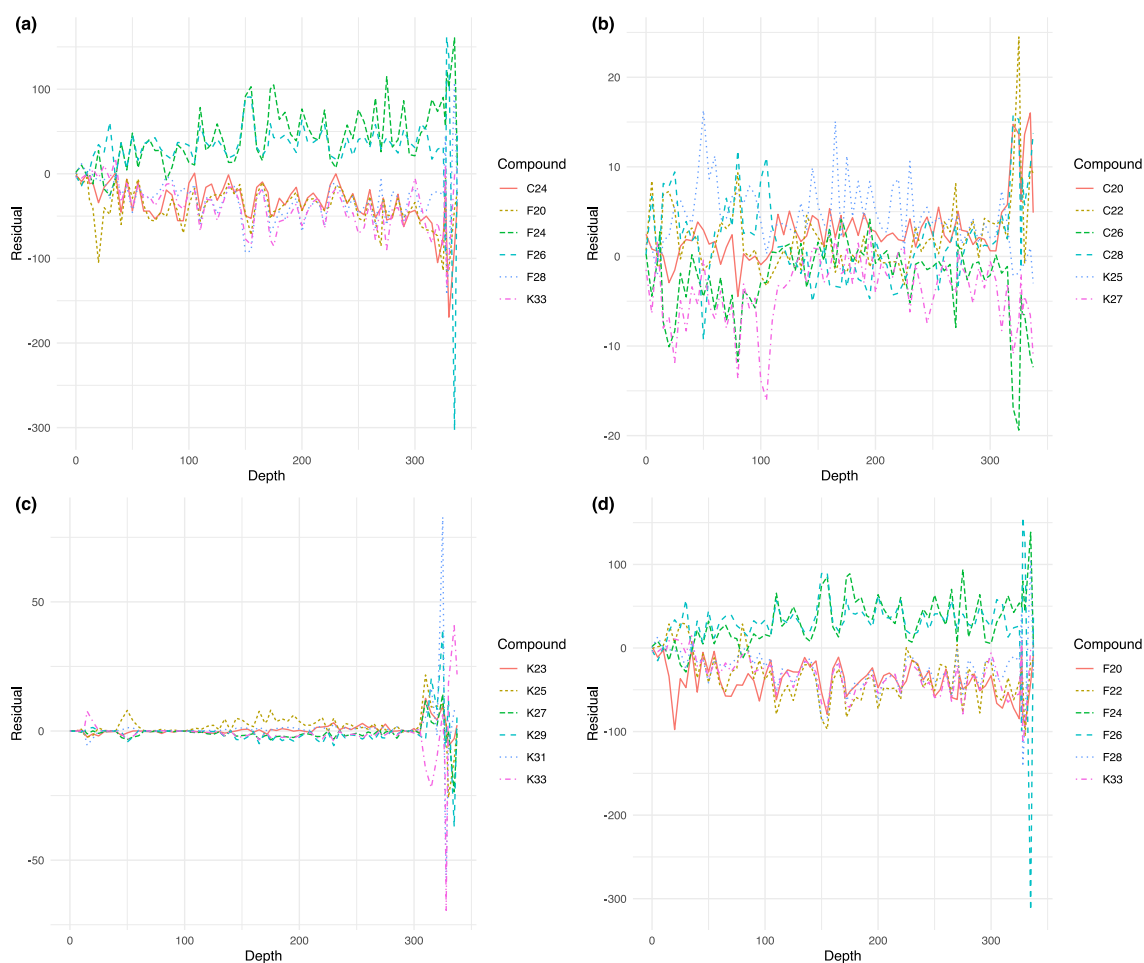


**Figure 11: Core measurement residuals versus depth for Run #13(a), Run #14 (b), Run #15 (c), and Run #16 (d), showing compounds with the highest residual values.**

## DISCUSSION

### BIOMARKER MEASUREMENTS IN MODERN PLANTS

The current species present at the Beerberg peatland generally represent an ombrotrophic bog in central Europe. Although previously published biomarker data is not available for all of the investigated plant species and parts, we could compare our data to those of a few studies.

Compared to the other *Sphagnum* mosses, *Sphagnum angustifolium* had a very high *n*-alkane concentration, contrasting previously published data from other locations (e.g., Vonk & Gustafsson, 2009 (Sweden)); additionally, *S. angustifolium* had an unexpectedly high  $P_{wax}$  value, likely due to  $C_{31}$  being the dominant chain length. This is also unexpected as previous studies have identified  $C_{23}$  (Bingham et al., 2010 (Finland)) and  $C_{27}/C_{29}$  (Vonk & Gustafsson, 2009 (Sweden)) as dominant chain lengths in *S. angustifolium*. The other

*Sphagnum* mosses (*S. capillifolium*, *S. fuscum*, and *S. magellanicum*) had lower *n*-alkane concentrations than measured at other locations (e.g., Vonk and Gustafsson, 2009 (subarctic Scandinavia). Furthermore, the  $P_{aq}$  values are lower than other published data (e.g., Vonk and Gustafsson, 2009). This is likely due to the dominance of  $C_{31}$  across all four of our measured species, which contrasts with other studies. *S. fuscum* has been reported as having  $C_{25}$  as a dominant chain length at sites in Ireland (Corrigan et al., 1973), Great Britain (Ficken et al., 1998), Finland (Bingham et al., 2010; Vonk & Gustafsson, 2009), and Sweden (Vonk & Gustafsson, 2009). *S. magellanicum* has more mixed results, with  $C_{25}$  reported as the dominant chain length at sites in the Netherlands (Baas et al., 2000), Ireland (Corrigan et al., 1973), Great Britain (Bingham et al., 2010), Finland (Bingham et al., 2010), and Sweden (Vonk & Gustafsson, 2009) and  $C_{31}$  the dominant chain length at sites in Denmark (Bingham et al., 2010) and Great Britain (Nott et al., 2000). *S. capillifolium* has also been reported in different studies as having either  $C_{25}$  (Vonk & Gustafsson, 2009; Sweden) or  $C_{31}$  (Nott et al., 2000; Ficken et al., 1998; Great Britain) as a dominant chain length. However, while  $C_{31}$  is not often the dominant chain length in *Sphagnum* mosses, it is often one of the chain lengths with higher concentrations, so our results still resemble typical *Sphagnum* distributions of *n*-alkanes. As mentioned, there is far less available data for *n*-alkanols and *n*-fatty acids. However, we found measurements for *S. fuscum*, *S. capillifolium*, and *S. magellanicum*. We found a dominant chain length of  $C_{26}$  *n*-alkanol for *S. fuscum* and  $C_{24}$  *n*-alkanol for *S. capillifolium*, which agrees with the findings of Ficken et al. (1998). Baas et al. 2000 found that *S. magellanicum* had a  $C_{26}$  *n*-alkanol dominant chain length, contrasting our findings of  $C_{24}$ . For the *n*-fatty acids, we found that each *Sphagnum* species had a dominant chain length of  $C_{24}$ , which agrees with findings for *S. fuscum* (Corrigan et al., 1976; Ficken et al., 1998) and *S. capillifolium* (Ficken et al. 1998). While Corrigan et al. 1976 also found a  $C_{24}$  dominant chain length for *S. magellanicum*, Baas et al., 2000 found  $C_{26}$ .

While we could find at least one published study with *n*-alkanes results for the shrub leaves, there is still a relative paucity of data for the compositions of stems and roots as well as for *n*-alkanols and *n*-fatty acids. *Calluna vulgaris* is a common plant in peatland settings and has been measured in multiple studies, with results that generally agree with ours. Salasoo measured *C. vulgaris* in both Germany (1987) and Austria (1989) at multiple altitudes, finding dominant chain lengths to be either  $C_{31}$  or  $C_{33}$ . Pancost et al. (2002) found that *C.*

*vulgaris* in the Netherlands had a  $C_{\max}$  in the leaves of 33, in a stem and leaves combination of  $C_{33}$ , and  $C_{31}$  in the roots. We found  $C_{31}$  dominant in the leaves and stems but  $C_{33}$  dominant in the roots. This causes a relatively high  $P_{\text{wax}}$  value for the roots, which could result in complications in interpreting peat cores. Pancost et al. (2002) also measured *n*-alkanols and *n*-fatty acids in *C. vulgaris*, finding  $C_{\max}$  of the *n*-alkanols to be  $C_{28}$  in the leaves, a bimodal  $C_{24}$  and  $C_{28}$  in the stems and leaves combination, and  $C_{24}$  in the roots and  $C_{\max}$  of the *n*-fatty acids to be  $C_{30}$  in the leaves,  $C_{24}$  in the stems and leaves, and  $C_{28}$  in the roots. The leaf results correspond with our findings, while the results of the stem and root measurements differ. Salasoo also measured *n*-alkanes in *V. myrtillus*, *V. uliginosum*, and *V. vitis-idaea* in both Germany (1987) and Austria (1989), as well as *O. palustris* in Austria (1989). Based on  $C_{\max}$  and  $ACL_{\text{ALK}}$ , the results are similar to our findings of *V. myrtillus* leaves having a dominant chain length of  $C_{31}$ , *V. uliginosum* having a  $C_{\max}$  of 27 (though in the Austrian samples, the  $C_{\max}$  was 25 (Salasoo, 1989)), and both *V. vitis-idaea* and *O. palustris* having a dominant chain length of  $C_{29}$ . Ficken et al. (1998) measured *n*-alkanes, *n*-alkanols, and *n*-fatty acids in *V. vitis-idaea* and *Empetrum nigrum*. The *n*-alkane results reflected ours, with *E. nigrum* having a relatively high *n*-alkane concentration as well as  $C_{31}$  as  $C_{\max}$  and *V. vitis-idaea* having  $C_{29}$  as  $C_{\max}$ . The *n*-alkanol results differed with Ficken et al. (1998), finding  $C_{30}$  as the  $C_{\max}$  for both species compared to our  $C_{26}$ . The *n*-fatty acid results for *E. nigrum* agree at  $C_{28}$  as  $C_{\max}$ , while those for *V. vitis-idaea* are very different, with Ficken et al. (1998) measuring  $C_{30}$  as the dominant chain length and our study finding  $C_{20}$ . Overall, the shrub results generally agreed with the previously published data we looked at, and the *n*-alkanes showed variation across species that seemed consistent across multiple locations.

Other studies have measured *n*-alkanes in coniferous needles, though results are limited for European settings. Maffei et al. (2004) found relatively low concentrations of *n*-alkanes in *P. sylvestris* and *P. abies* needles, as well as  $C_{\max}$  of  $C_{31}$  in both species. In our study, we found  $C_{29}$  as the  $C_{\max}$  for both.

Our results from the biomarker analysis of the modern plant samples show that signatures across plant groups and parts exhibit some overlap, as found in previous studies. This increases the difficulty of organic matter source apportionment based on biomarker distributions. In our assemblage of plants, the most potentially problematic overlaps occurred in the *n*-alkane measurements and ratios. The  $C_{23}/C_{25}$  ratio has been previously

suggested to be connected to bog wetness as it has been observed that *Sphagnum* species occupying drier hummock habitats (e.g., *S. fuscum* and *S. capillifolium* are dominated by higher chain lengths such as C<sub>25</sub> or C<sub>31</sub>, while species in wetter hollow habitats are dominated by C<sub>23</sub> (Bingham et al., 2010). Our study found that all the *Sphagnum* mosses were dominated by C<sub>31</sub>, meaning that the C<sub>23</sub>/C<sub>25</sub> ratio is likely less effective at the Beerberg peatland. C<sub>31</sub> is also used in the P<sub>aq</sub> and P<sub>wax</sub> ratios, and the unexpected dominance of C<sub>31</sub> in *Sphagnum* mosses and some of the root samples likely contributed to a few of the unexpected results for the two ratios that would make it difficult to determine biomarker inputs accurately based only on the ratios. However, the P<sub>aq</sub> and P<sub>wax</sub> ratios were important contributors to variance in the PCAs of both the plant samples and the core samples, along with the C<sub>25</sub>/(C<sub>25</sub>+C<sub>29</sub>) ratio. Our results confirm the importance of having a localized library of plant biomarker data to compare to sedimentary archives, as well as to include a variety of index measurements or ratios in case the local biomarker signatures of the plants render the ratios less effective.

## EVALUATING THE VERHIB MODEL RECONSTRUCTION

The VERHIB model results provide insight into the modeling process and the biomarker data. All the runs struggled to capture an accurate representation of the transitions seen not only in the plant macrofossil records but also with temporal offsets in the pollen record and the core elemental and biomarker data (Thomas et al., 2023b). Based on the plant macrofossils, four phases were identified: 2528-2251 cal yr BP (340-318.5 cm), 2251-1671 cal yr BP (318.5-273.5 cm), 1671-64 cal yr BP (273.5-15.5 cm), and 64 cal yr BP - Present (15.5-0 cm). In Phase I, the vegetation was predominately poor fen before going through paludification and transitioning to a *Sphagnum* bog in Phase II. The peatland was relatively stable through Phase III until Phase IV, when there was an increase in some fen species like *E. vaginatum* and a change in dominant *Sphagnum* species from *S. fuscum* to *S. medium/divinum*.

The reconstructions closest to the plant macrofossil record included all chain lengths and *n*-fatty acids (Runs #1, #4, #5, #8) (Figs. 4a, 4d, 6a, 6d). These reconstructions correctly estimated that *S. fuscum* was the dominant moss through most of the core, transitioning only in the last phase to a different species. Additionally, these reconstructions showed a higher proportion of Ericaceae shrubs at the bottom of the core and closer to the top. However, the

proportion of *E. vaginatum* was underestimated, particularly at the base of the core, potentially causing the higher residuals at lower depths (Figs. 5a, 5d, 7a, 7d). When only plant-derived chain lengths were included, *S. fuscum* was not recognized as the dominant moss, and when *n*-fatty acid data was excluded, the proportion of tree species was overestimated. The VERHIB model was previously only used with *n*-alkane and *n*-alkanol data, so this is the first time that *n*-fatty acid data has been shown to be a valuable inclusion. In these reconstructions, including root data did not alter the result significantly, but this is logical as the peatland vegetation was dominated by *Sphagnum* moss, and there was likely not a lot of root input from other plants.

We additionally considered the Pearson correlation coefficients between the predicted peat core biomarker values and the actual values. What we found echoed the importance of including *n*-fatty acid data and all chain lengths, not only plant-derived. The Pearson correlation coefficients were over 0.9 for all model runs except #1, #4, and #5. This result shows that these runs were overparameterized and that the model could be solved with a non-unique solution.

Although the VERHIB reconstructions were not wholly accurate, particularly in failing to identify the poor fen vegetation present in Phase I, the results are still promising and provide some insight into how the model might be adapted in future research.

## FUTURE RECOMMENDATIONS FOR THE VERHIB MODEL

There are a few opportunities for improving the VERHIB model that could increase its accuracy and applicability to more study sites, as well as its usability for a wider group of researchers. As MATLAB requires a license, developing a version of the VERHIB model in R would allow for more widespread use as R is open-source and more prevalent today in ecological and environmental research. An R version could be more easily expandable to include further compound classes, such as the *n*-fatty acids we tested here.

Another potential improvement for the model would be the addition of a module allowing plant macrofossil or pollen data to be considered. As seen in Fig. 12, there are a lot of overlaps between current vegetation species found at the peatland and those within the plant macrofossil record. The pollen record contains many other species, but this is not

unexpected as pollen is typically airborne, and the record is therefore a regional rather than local signal. Other models using biomarkers have been more recently developed with Bayesian approaches (Yang and Bowen, 2022) that allow for consideration of prior knowledge to inform the final estimate. Our study shows that many species and plant parts have overlapping biomarker signatures that complicate the source apportionment process. If the model had access to other proxy data in the form of plant macrofossils or pollen, the biomarker-based reconstruction could be better informed by which species are more likely to have been present at different points in time. There has also been promising research into using machine learning techniques with biomarker data from lake sediments (Peaple et al., 2021), and this could be an additional avenue for improvement of the VERHIB model following the development of a more widely accessible version.

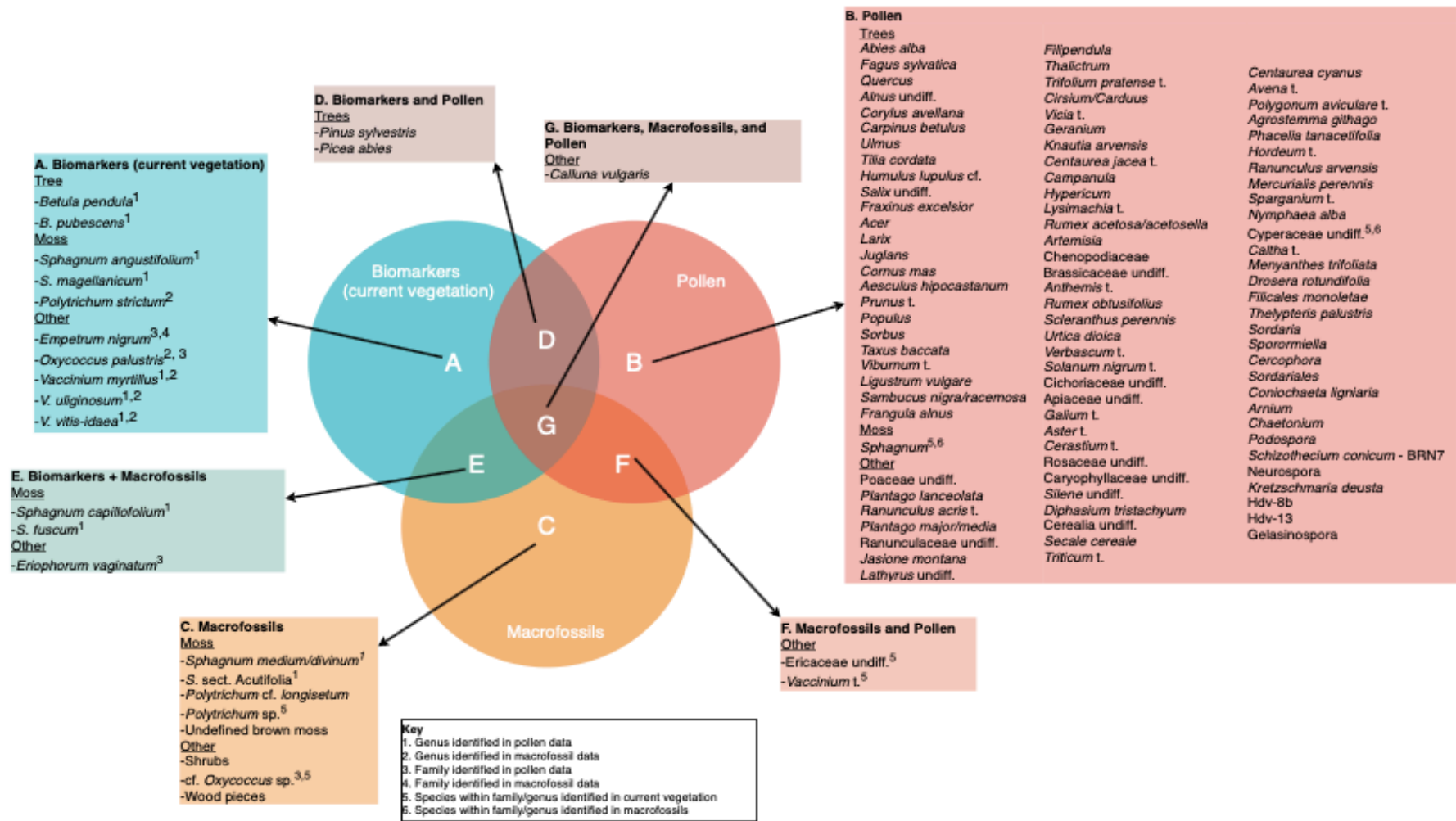


Figure 12: Comparison of species present in current vegetation at Beerberg peatland with those found in the plant macrofossil and pollen records.

## CONCLUSION

Our study echoes what has been found before, that while biomarkers can serve as a proxy for paleovegetation and paleoclimate conditions, on their own, they are often not precise enough and work best when augmented by other proxies, such as pollen or macrofossils. The lack of precision results from overlapping biomarker signatures across plant species and plant organs, as well as the inherent uncertainty of using modern plant analogues to evaluate source apportionment for past vegetation growing under likely different climate conditions. A potential next step for increasing the rigor and quantitiveness of multi-proxy studies using biomarkers would be to create a model capable of integrating plant macrofossil or pollen data into a biomarker-based reconstruction to allow for more probable outcomes.

Additionally, it is essential to develop a library of plant biomarker signatures that is as localized as possible to the site under investigation. Furthermore, an easily accessible database of published plant biomarker signatures will enable researchers to better choose if they need to analyze plants at their site or if sufficient data is available from plant species in the region. This could also allow for a better understanding of how climate and environmental variables affect biomarker signatures, enabling the possibility of correcting for climate changes over time when using modern plant analogues for a paleoreconstruction.

## REFERENCES

- Andersson, R. A., Kuhry, P., Meyers, P., Zebühr, Y., Crill, P., & Mörth, M. (2011). Impacts of paleohydrological changes on *n*-alkane biomarker compositions of a Holocene peat sequence in the eastern European Russian Arctic. *Organic Geochemistry*, 42(9), 1065–1075. <https://doi.org/10.1016/j.orggeochem.2011.06.020>
- Baas, M., Pancost, R., Van Geel, B., & Sinninghe Damsté, J. S. (2000). A comparative study of lipids in *Sphagnum* species. *Organic Geochemistry*, 31(6), 535–541. [https://doi.org/10.1016/S0146-6380\(00\)00037-1](https://doi.org/10.1016/S0146-6380(00)00037-1)
- Bingham, E. M., McClymont, E. L., Väiliranta, M., Mauquoy, D., Roberts, Z., Chambers, F. M., Pancost, R. D., & Evershed, R. P. (2010). Conservative composition of *n*-alkane biomarkers in *Sphagnum* species: Implications for palaeoclimate reconstruction in ombrotrophic peat bogs. *Organic Geochemistry*, 41(2), 214–220. <https://doi.org/10.1016/j.orggeochem.2009.06.010>
- Birks, H. H., & Birks, H. J. B. (2000). Future uses of pollen analysis must include plant macrofossils. *Journal of Biogeography*, 27(1), 31–35.
- Corrigan, D., Kloos, C., O'Connor, C. S., & Timoney, R. F. (1973). Alkanes from four species of *Sphagnum* moss. *Phytochemistry*, 12(1), 213–214. [https://doi.org/10.1016/S0031-9422\(00\)84653-1](https://doi.org/10.1016/S0031-9422(00)84653-1)

- Corrigan, D., Kloos, C., O'Connor, C., & Timoney, R. (1976). Lipid components of *Sphagnum* mosses. *Planta Medica*, 29(03), 261–267. <https://doi.org/10.1055/s-0028-1097660>
- Cranwell, P. A. (1974). Monocarboxylic acids in lake sediments: Indicators, derived from terrestrial and aquatic biota, of paleoenvironmental trophic levels. *Chemical Geology*, 14(1), 1–14. [https://doi.org/10.1016/0009-2541\(74\)90092-8](https://doi.org/10.1016/0009-2541(74)90092-8)
- Cranwell, P. A. (1981). Diagenesis of free and bound lipids in terrestrial detritus deposited in a lacustrine sediment. *Organic Geochemistry*, 3(3), 79–89. [https://doi.org/10.1016/0146-6380\(81\)90002-4](https://doi.org/10.1016/0146-6380(81)90002-4)
- Crausbay, S., Genderjahn, S., Hotchkiss, S., Sachse, D., Kahmen, A., & Arndt, S. K. (2014). Vegetation dynamics at the upper reaches of a tropical montane forest are driven by disturbance over the past 7300 years. *Arctic, Antarctic, and Alpine Research*, 46(4), 787–799. <https://doi.org/10.1657/1938-4246-46.4.787>
- Eglinton, G., & Hamilton, R. J. (1967). Leaf epicuticular waxes. *Science*, 156, 1322–1335.
- Erb, K.-H., Kastner, T., Plutzer, C., Bais, A. L. S., Carvalhais, N., Fetzl, T., Gingrich, S., Haberl, H., Lauk, C., Niedertscheider, M., Pongratz, J., Thurner, M., & Luysaert, S. (2018). Unexpectedly large impact of forest management and grazing on global vegetation biomass. *Nature*, 553(7686), 73–76. <https://doi.org/10.1038/nature25138>
- Ficken, K. J., Barber, K. E., & Eglinton, G. (1998). Lipid biomarker,  $\delta^{13}\text{C}$  and plant macrofossil stratigraphy of a Scottish montane peat bog over the last two millennia. *Organic Geochemistry*, 28(3), 217–237. [https://doi.org/10.1016/S0146-6380\(97\)00126-5](https://doi.org/10.1016/S0146-6380(97)00126-5)
- Ficken, K. J., Li, B., Swain, D. L., & Eglinton, G. (2000). An *n*-alkane proxy for the sedimentary input of submerged/floating freshwater aquatic macrophytes. *Organic Geochemistry*, 31(7), 745–749. [https://doi.org/10.1016/S0146-6380\(00\)00081-4](https://doi.org/10.1016/S0146-6380(00)00081-4)
- Gocke, M., Kuzyakov, Y., & Wiesenberg, G. L. B. (2010). Rhizoliths in loess – evidence for post-sedimentary incorporation of root-derived organic matter in terrestrial sediments as assessed from molecular proxies. *Organic Geochemistry*, 41(11), 1198–1206. <https://doi.org/10.1016/j.orggeochem.2010.08.001>
- Hirave, P., Wiesenberg, G. L. B., Birkholz, A., & Alewell, C. (2020). Understanding the effects of early degradation on isotopic tracers: Implications for sediment source attribution using compound-specific isotope analysis (CSIA). *Biogeosciences*, 17(8), 2169–2180. <https://doi.org/10.5194/bg-17-2169-2020>
- Husson, F., Josse, J., Le, S., & Mazet, J. (2023). *FactoMineR: Multivariate Exploratory Data Analysis and Data Mining* (2.8) [Computer software]. <https://cran.r-project.org/web/packages/FactoMineR/index.html>
- Jackson, R. B., Lajtha, K., Crow, S. E., Hugelius, G., Kramer, M. G., & Piñeiro, G. (2017). The ecology of soil carbon: Pools, vulnerabilities, and biotic and abiotic controls. *Annual Review of Ecology, Evolution, and Systematics*, 48(1), 419–445. <https://doi.org/10.1146/annurev-ecolsys-112414-054234>
- Jansen, B., De Boer, E. J., Cleef, A. M., Hooghiemstra, H., Moscol-Olivera, M., Tonneijck, F. H., & Verstraten, J. M. (2013). Reconstruction of late Holocene forest dynamics in northern Ecuador from

- biomarkers and pollen in soil cores. *Palaeogeography, Palaeoclimatology, Palaeoecology*, 386, 607–619. <https://doi.org/10.1016/j.palaeo.2013.06.027>
- Jansen, B., Nierop, K. G. J., Hageman, J. A., Cleef, A. M., & Verstraten, J. M. (2006). The straight-chain lipid biomarker composition of plant species responsible for the dominant biomass production along two altitudinal transects in the Ecuadorian Andes. *Organic Geochemistry*, 37(11), 1514–1536. <https://doi.org/10.1016/j.orggeochem.2006.06.018>
- Jansen, B., Van Loon, E. E., Hooghiemstra, H., & Verstraten, J. M. (2010). Improved reconstruction of palaeoenvironments through unravelling of preserved vegetation biomarker patterns. *Palaeogeography, Palaeoclimatology, Palaeoecology*, 285(1–2), 119–130. <https://doi.org/10.1016/j.palaeo.2009.10.029>
- Jansen, B., & Wiesenberg, G. L. B. (2017). Opportunities and limitations related to the application of plant-derived lipid molecular proxies in soil science. *SOIL*, 3(4), 211–234. <https://doi.org/10.5194/soil-3-211-2017>
- Kassambara, A., & Mundt, F. (2020). *factoextra: Extract and Visualize the Results of Multivariate Data Analyses* (1.0.7) [Computer software]. <https://cran.r-project.org/web/packages/factoextra/index.html>
- Lavorel, S., Díaz, S., Cornelissen, J. H. C., Garnier, E., Harrison, S. P., McIntyre, S., Pausas, J. G., Pérez-Harguindeguy, N., Roumet, C., & Urcelay, C. (2007). Plant Functional Types: Are We Getting Any Closer to the Holy Grail? In J. G. Canadell, D. E. Pataki, & L. F. Pitelka (Eds.), *Terrestrial Ecosystems in a Changing World* (pp. 149–164). Springer Berlin Heidelberg. [https://doi.org/10.1007/978-3-540-32730-1\\_13](https://doi.org/10.1007/978-3-540-32730-1_13)
- Lavrieux, M., Bréheret, J.G., Disnar, J.R., Jacob, J., Le Milbeau, C., Zocatelli, R. (2012). Preservation of an ancient grassland biomarker signature in a forest soil from the French Massif Central. *Organic Geochemistry* 51, 1–10. doi:10.1016/j.orggeochem.2012.07.003.
- Maffei, M., Badino, S., & Bossi, S. (2004). Chemotaxonomic significance of leaf wax *n*-alkanes in the *Pinales* (*Coniferales*). *Journal of Biological Research*, 1, 3-19.
- Marzi, R., Torkelson, B. E., & Olson, R. K. (1993). A revised carbon preference index. *Organic Geochemistry*, 20(8), 1303–1306. [https://doi.org/10.1016/0146-6380\(93\)90016-5](https://doi.org/10.1016/0146-6380(93)90016-5)
- McClymont, E. L., Mauquoy, D., Yeloff, D., Broekens, P., van Geel, B., Charman, D. J., Pancost, R. D., Chambers, F. M., & Evershed, R. P. (2008). The disappearance of *Sphagnum imbricatum* from Butterburn Flow, UK. *The Holocene*, 18(6), 991–1002. <https://doi.org/10.1177/0959683608093537>
- Nott, C. J., Xie, S., Avsejs, L. A., Maddy, D., Chambers, F. M., & Evershed, R. P. (2000). *n*-Alkane distributions in ombrotrophic mires as indicators of vegetation change related to climatic variation. *Organic Geochemistry*, 31(2), 231–235. [https://doi.org/10.1016/S0146-6380\(99\)00153-9](https://doi.org/10.1016/S0146-6380(99)00153-9)
- Parducci, L., Väiliranta, M., Salonen, J. S., Ronkainen, T., Matetovici, I., Fontana, S. L., Eskola, T., Sarala, P., Suyama, Y. (2015). Proxy comparison in ancient peat sediments: pollen, macrofossil and plant DNA. *Philosophical Transactions of the Royal Society B: Biological Sciences* 370, 20130382. <https://doi.org/10.1098/rstb.2013.0382>

- Pancost, R. D., Baas, M., van Geel, B., & Sinninghe Damsté, J. S. (2002). Biomarkers as proxies for plant inputs to peats: An example from a sub-boreal ombrotrophic bog. *Organic Geochemistry*, 33(7), 675–690. [https://doi.org/10.1016/S0146-6380\(02\)00048-7](https://doi.org/10.1016/S0146-6380(02)00048-7)
- Peuple, M. D., Tierney, J. E., McGee, D., Lowenstein, T. K., Bhattacharya, T., & Feakins, S. J. (2021). Identifying plant wax inputs in lake sediments using machine learning. *Organic Geochemistry*, 156, 104222. <https://doi.org/10.1016/j.orggeochem.2021.104222>
- Peters, K. E., Walters, C. C., & Moldowan, J. M. (2005). *The Biomarker Guide*. Cambridge University Press.
- Poynter, J. G., Farrimond, P., Robinson, N., & Eglinton, G. (1989). Aeolian-Derived Higher Plant Lipids in the Marine Sedimentary Record: Links with Palaeoclimate. In M. Leinen & M. Sarnthein (Eds.), *Paleoclimatology and Paleometeorology: Modern and Past Patterns of Global Atmospheric Transport* (pp. 435–462). Springer Netherlands. [https://doi.org/10.1007/978-94-009-0995-3\\_18](https://doi.org/10.1007/978-94-009-0995-3_18)
- Ronkainen, T., McClymont, E. L., Väiliranta, M., & Tuittila, E.-S. (2013). The *n*-alkane and sterol composition of living fen plants as a potential tool for palaeoecological studies. *Organic Geochemistry*, 59, 1–9. <https://doi.org/10.1016/j.orggeochem.2013.03.005>
- Salasoo, I. (1987). Epicuticular wax hydrocarbons of Ericaceae in Germany. *Zeitschrift Für Naturforschung C*, 42(5), 499–501. <https://doi.org/10.1515/znc-1987-0501>
- Salasoo, I. (1989). Epicuticular wax alkanes of Ericaceae and *Empetrum* from alpine and sub-alpine heaths in Austria. *Plant Systematics and Evolution*, 163(1–2), 71–79. <https://doi.org/10.1007/BF00936154>
- Schmidt, M. W. I., Torn, M. S., Abiven, S., Dittmar, T., Guggenberger, G., Janssens, I. A., Kleber, M., Kögel-Knabner, I., Lehmann, J., Manning, D. A. C., Nannipieri, P., Rasse, D. P., Weiner, S., & Trumbore, S. E. (2011). Persistence of soil organic matter as an ecosystem property. *Nature*, 478(7367), 49–56. <https://doi.org/10.1038/nature10386>
- Srivastava, K., & Wiesenberg, G. L. B. (2018). Severe drought-influenced composition and  $\delta^{13}\text{C}$  of plant and soil *n*-alkanes in model temperate grassland and heathland ecosystems. *Organic Geochemistry*, 116, 77–89. <https://doi.org/10.1016/j.orggeochem.2017.11.002>
- Thomas, C. L., Jansen, B., Czerwiński, S., Gałka, M., Knorr, K.-H., Van Loon, E. E., Egli, M., & Wiesenberg, G. L. B. (2023a). Comparison of paleobotanical and biomarker records of mountain peatland and forest ecosystem dynamics over the last 2600 years in central Germany. *Biogeosciences*, 20, 4893–4914. <https://doi.org/10.5194/bg-20-4893-2023>
- Thomas, C. L., Jansen, B., Czerwiński, S., Gałka, M., Knorr, K.-H., van Loon, E. E., Egli, M., Wiesenberg, G. L. B. (2023b). Paleobotanical and biomarker records over 2600 years from Beerberg peatland (Central Germany). <https://doi.org/10.1594/PANGAEA.961142>, doi:10.1594/PANGAEA.961142. type: data set.
- Thomas, C. L., Jansen, B., Van Loon, E. E., & Wiesenberg, G. L. B. (2021). Transformation of *n*-alkanes from plant to soil: A review. *SOIL*, 7(2), 785–809. <https://doi.org/10.5194/soil-7-785-2021>
- Van Mourik, J. M., & Jansen, B. (2013). The added value of biomarker analysis in palaeopedology; reconstruction of the vegetation during stable periods in a polycyclic driftsand sequence in SE-Netherlands. *Quaternary International*, 306, 14–23. <https://doi.org/10.1016/j.quaint.2013.05.034>

- Van Mourik, J. M., Wagner, T. V., De Boer, J. G., & Jansen, B. (2016). The added value of biomarker analysis to the genesis of plagic Anthrosols; the identification of stable fillings used for the production of plagic manure. *SOIL*, 2(3), 299–310. <https://doi.org/10.5194/soil-2-299-2016>
- Vonk, J. E., & Gustafsson, Ö. (2009). Calibrating *n*-alkane *Sphagnum* proxies in sub-Arctic Scandinavia. *Organic Geochemistry*, 40(10), 1085–1090. <https://doi.org/10.1016/j.orggeochem.2009.07.002>
- Wiesenberg, G. L. B., & Gocke, M. I. (2015). Analysis of Lipids and Polycyclic Aromatic Hydrocarbons as Indicators of Past and Present (Micro)Biological Activity. In T. J. McGenity, K. N. Timmis, & B. Nogales (Eds.), *Hydrocarbon and Lipid Microbiology Protocols* (pp. 61–91). Springer Berlin Heidelberg. [https://doi.org/10.1007/8623\\_2015\\_157](https://doi.org/10.1007/8623_2015_157)
- Wüthrich, L., Bliedtner, M., Schäfer, I., Zech, J., Shajari, F., Gaar, D., Preusser, F., Salazar, G., Szidat, S., & Zech, R. (2017). Late Quaternary climate and environmental reconstruction based on leaf wax analyses in the loess sequence of Möhlin, Switzerland. *E&G Quaternary Science Journal*, 66. <https://doi.org/10.5194/egqsj-66-91-2017>
- Yang, D., & Bowen, G. J. (2022). Integrating plant wax abundance and isotopes for paleo-vegetation and paleoclimate reconstructions: A multi-source mixing model using a Bayesian framework. *Climate of the Past*, 18(10), 2181–2210. <https://doi.org/10.5194/cp-18-2181-2022>
- Zheng, Y., Zhou, W., Liu, Z., & Liu, X. (2011). The *n*-alkanol paleoclimate records in two peat deposits: A comparative study of the northeastern margin of the Tibetan Plateau and Northeast China. *Environmental Earth Sciences*, 63(1), 135–143. <https://doi.org/10.1007/s12665-010-0676-2>
- Zheng, Y., Zhou, W., Meyers, P. A., & Xie, S. (2007). Lipid biomarkers in the Zoigê-Hongyuan peat deposit: Indicators of Holocene climate changes in West China. *Organic Geochemistry*, 38(11), 1927–1940. <https://doi.org/10.1016/j.orggeochem.2007.06.012>
- Zhou, W., Xie, S., Meyers, P. A., & Zheng, Y. (2005). Reconstruction of late glacial and Holocene climate evolution in southern China from geolipids and pollen in the Dingnan peat sequence. *Organic Geochemistry*, 36(9), 1272–1284. <https://doi.org/10.1016/j.orggeochem.2005.04.005>

**Table S1. Extra model runs.**

Run #	Compounds included	Species included	Leaf:root ratio	Reg (depth)	Reg (group)	Max iterations	Pearson coefficient (soil chem values)
S1	ALC: C <sub>15</sub> -C <sub>28</sub> ,	All; group 1: <i>S. angustifolium</i> , <i>S. magellanicum</i> , <i>S. capillifolium</i> , <i>S. fuscum</i> , group 2: <i>C. vulgaris</i> , <i>V. uliginosum</i> , <i>V. myrtillus</i> , <i>V. vitis-idaea</i> , <i>O. palustris</i> , <i>E. nigrum</i> , group 3: <i>E. vaginatum</i> , group 4: <i>P. strictum</i> , group 5: <i>P. sylvestris</i> , group 6: <i>P. abies</i> , group 7: <i>B. pendula</i> , <i>B. pubescens</i>	1:0	0.1	0.1	2000	0.997311
S2	FA: C <sub>14</sub> -C <sub>32</sub>	All; group 1: <i>S. angustifolium</i> , <i>S. magellanicum</i> , <i>S. capillifolium</i> , <i>S. fuscum</i> , group 2: <i>C. vulgaris</i> , <i>V. uliginosum</i> , <i>V. myrtillus</i> , <i>V. vitis-idaea</i> , <i>O. palustris</i> , <i>E. nigrum</i> , group 3: <i>E. vaginatum</i> , group 4: <i>P. strictum</i> , group 5: <i>P. sylvestris</i> , group 6: <i>P. abies</i> , group 7: <i>B. pendula</i> , <i>B. pubescens</i>	1:0	0.1	0.1	2000	0.68894
S3	ALC: C <sub>15</sub> -C <sub>28</sub> , FA: C <sub>14</sub> -C <sub>32</sub>	All; group 1: <i>S. angustifolium</i> , <i>S. magellanicum</i> , <i>S. capillifolium</i> , <i>S. fuscum</i> , group 2: <i>C. vulgaris</i> , <i>V. uliginosum</i> , <i>V. myrtillus</i> , <i>V. vitis-idaea</i> , <i>O. palustris</i> , <i>E. nigrum</i> , group 3: <i>E. vaginatum</i> , group 4: <i>P. strictum</i> , group 5: <i>P. sylvestris</i> , group 6: <i>P. abies</i> , group 7: <i>B. pendula</i> , <i>B. pubescens</i>	1:0	0.1	0.1	2000	0.71656
S4	All; ALK: C <sub>19</sub> -C <sub>33</sub> , ALC: C <sub>15</sub> -C <sub>28</sub> , FA: C <sub>14</sub> -C <sub>32</sub>	group 1: <i>S. angustifolium</i> , <i>S. magellanicum</i> , <i>S. capillifolium</i> , <i>S. fuscum</i> , group 2: <i>C. vulgaris</i> , <i>V. uliginosum</i> , <i>V. myrtillus</i> , <i>V. vitis-idaea</i> , <i>O. palustris</i> , <i>E. nigrum</i> , group 3: <i>E. vaginatum</i> , group 4: <i>P. strictum</i>	5:1	0.2	0.1	2000	0.743593
S5	All; ALK: C <sub>19</sub> -C <sub>33</sub> , ALC: C <sub>15</sub> -C <sub>28</sub> , FA: C <sub>14</sub> -C <sub>32</sub>	group 1: <i>S. angustifolium</i> , <i>S. magellanicum</i> , <i>S. capillifolium</i> , <i>S. fuscum</i> , group 2: <i>C. vulgaris</i> , <i>V. uliginosum</i> , <i>V. myrtillus</i> , <i>V. vitis-idaea</i> , <i>O. palustris</i> , <i>E. nigrum</i> , group 3: <i>E. vaginatum</i> , group 4: <i>P. strictum</i>	5:1	0.1	0.1	2000	0.743593
S6	All; ALK: C <sub>19</sub> -C <sub>33</sub> , ALC: C <sub>15</sub> -C <sub>28</sub> , FA: C <sub>14</sub> -C <sub>32</sub>	group 1: <i>S. angustifolium</i> , <i>S. magellanicum</i> , <i>S. capillifolium</i> , <i>S. fuscum</i> , group 2: <i>C. vulgaris</i> , <i>V. uliginosum</i> , <i>V. myrtillus</i> , <i>V. vitis-idaea</i> , <i>O. palustris</i> , <i>E. nigrum</i> , group 3: <i>E. vaginatum</i> , group 4: <i>P. strictum</i>	5:1	0.2	0.1	2000	0.743593
S7	Plant-derived; ALK, ALC	All; group 1: <i>S. angustifolium</i> , <i>S. magellanicum</i> , <i>S. capillifolium</i> , <i>S. fuscum</i> , group 2: <i>C. vulgaris</i> , <i>V.</i>	5:1	0.5	0.1	2000	0.997095

		<i>uliginosum</i> , <i>V. myrtillus</i> , <i>V. vitis-idaea</i> , <i>O. palustris</i> , <i>E. nigrum</i> , group 3: <i>E. vaginatum</i> , group 4: <i>P. strictum</i> , group 5: <i>P. sylvestris</i> , group 6: <i>P. abies</i> , group 7: <i>B. pendula</i> , <i>B. pubescens</i>					
S8	Plant-derived; ALK, ALC	All; group 1: <i>S. angustifolium</i> , <i>S. capillifolium</i> , group 2: <i>S. magellanicum</i> , <i>S. fuscum</i> , group 3: <i>C. vulgaris</i> , <i>V. uliginosum</i> , <i>V. myrtillus</i> , <i>V. vitis-idaea</i> , <i>O. palustris</i> , <i>E. nigrum</i> , <i>E. vaginatum</i> , group 4: <i>P. strictum</i> , group 5: <i>P. sylvestris</i> , group 6: <i>P. abies</i> , group 7: <i>B. pendula</i> , <i>B. pubescens</i>	5:1	0.5	0.1	2000	0.996989
S9	Plant-derived; ALK, ALC	All; group 1: <i>S. angustifolium</i> , <i>S. capillifolium</i> , group 2: <i>S. magellanicum</i> , <i>S. fuscum</i> , group 3: <i>C. vulgaris</i> , <i>Vaccinium uliginosum</i> , <i>V. myrtillus</i> , <i>V. vitis-idaea</i> , <i>Oxycoccus palustris</i> , <i>Empetrum nigrum</i> , <i>E. vaginatum</i> , group 4: <i>P. strictum</i> , group 5: <i>P. sylvestris</i> , group 6: <i>P. abies</i> , group 7: <i>B. pendula</i> , <i>B. pubescens</i>	5:1	0.5	0.5	2000	0.996987
S10	Plant-derived; ALK, ALC	All; group 1: <i>S. angustifolium</i> , <i>S. capillifolium</i> , group 2: <i>S. magellanicum</i> , <i>S. fuscum</i> , group 3: <i>C. vulgaris</i> , <i>V. uliginosum</i> , <i>V. myrtillus</i> , <i>V. vitis-idaea</i> , <i>O. palustris</i> , <i>E. nigrum</i> , <i>E. vaginatum</i> , group 4: <i>P. strictum</i> , group 5: <i>P. sylvestris</i> , group 6: <i>P. abies</i> , group 7: <i>B. pendula</i> , <i>B. pubescens</i>	3:1	0.5	0.5	2000	0.996995
S11	Plant-derived; ALK	All; group 1: <i>S. angustifolium</i> , <i>S. capillifolium</i> , group 2: <i>S. magellanicum</i> , <i>S. fuscum</i> , group 3: <i>C. vulgaris</i> , <i>V. uliginosum</i> , <i>V. myrtillus</i> , <i>V. vitis-idaea</i> , <i>O. palustris</i> , <i>E. nigrum</i> , <i>E. vaginatum</i> , group 4: <i>P. strictum</i> , group 5: <i>P. sylvestris</i> , group 6: <i>P. abies</i> , group 7: <i>B. pendula</i> , <i>B. pubescens</i>	3:1	0.5	0.5	2000	0.999522
S12	Plant-derived; ALK, ALC, FA	All; group 1: <i>S. angustifolium</i> , <i>S. magellanicum</i> , <i>S. capillifolium</i> , <i>S. fuscum</i> , group 2: <i>C. vulgaris</i> , <i>V. uliginosum</i> , <i>V. myrtillus</i> , <i>V. vitis-idaea</i> , <i>O. palustris</i> , <i>E. nigrum</i> , group 3: <i>E. vaginatum</i> , group 4: <i>P. strictum</i> , group 5: <i>P. sylvestris</i> , group 6: <i>P. abies</i> , group 7: <i>B. pendula</i> , <i>B. pubescens</i>	1:0	0.1	0.1	2000	0.978307
S13	Plant-derived; ALK, ALC	All; group 1: <i>S. angustifolium</i> , <i>S. magellanicum</i> , <i>S. capillifolium</i> , <i>S. fuscum</i> , group 2: <i>C. vulgaris</i> , <i>V.</i>	1:0	0.1	0.1	2000	0.997224

		<i>uliginosum</i> , <i>V. myrtillus</i> , <i>V. vitis-idaea</i> , <i>O. palustris</i> , <i>E. nigrum</i> , group 3: <i>E. vaginatum</i> , group 4: <i>P. strictum</i> , group 5: <i>P. sylvestris</i> , group 6: <i>P. abies</i> , group 7: <i>B. pendula</i> , <i>B. pubescens</i>					
S14	Plant-derived; ALK	All; group 1: <i>S. angustifolium</i> , <i>S. magellanicum</i> , <i>S. capillifolium</i> , <i>S. fuscum</i> , group 2: <i>C. vulgaris</i> , <i>V. uliginosum</i> , <i>V. myrtillus</i> , <i>V. vitis-idaea</i> , <i>O. palustris</i> , <i>E. nigrum</i> , group 3: <i>E. vaginatum</i> , group 4: <i>P. strictum</i> , group 5: <i>P. sylvestris</i> , group 6: <i>P. abies</i> , group 7: <i>B. pendula</i> , <i>B. pubescens</i>	1:0	0.1	0.1	2000	0.999522
S15	Plant-derived; ALC	All; group 1: <i>S. angustifolium</i> , <i>S. magellanicum</i> , <i>S. capillifolium</i> , <i>S. fuscum</i> , group 2: <i>C. vulgaris</i> , <i>V. uliginosum</i> , <i>V. myrtillus</i> , <i>V. vitis-idaea</i> , <i>O. palustris</i> , <i>E. nigrum</i> , group 3: <i>E. vaginatum</i> , group 4: <i>P. strictum</i> , group 5: <i>P. sylvestris</i> , group 6: <i>P. abies</i> , group 7: <i>B. pendula</i> , <i>B. pubescens</i>	1:0	0.1	0.1	2000	0.999004
S16	Plant-derived; FA	All; group 1: <i>S. angustifolium</i> , <i>S. magellanicum</i> , <i>S. capillifolium</i> , <i>S. fuscum</i> , group 2: <i>C. vulgaris</i> , <i>V. uliginosum</i> , <i>V. myrtillus</i> , <i>V. vitis-idaea</i> , <i>O. palustris</i> , <i>E. nigrum</i> , group 3: <i>E. vaginatum</i> , group 4: <i>P. strictum</i> , group 5: <i>P. sylvestris</i> , group 6: <i>P. abies</i> , group 7: <i>B. pendula</i> , <i>B. pubescens</i>	1:0	0.1	0.1	2000	0.987176
S17	Plant-derived; ALC, FA	All; group 1: <i>S. angustifolium</i> , <i>S. magellanicum</i> , <i>S. capillifolium</i> , <i>S. fuscum</i> , group 2: <i>C. vulgaris</i> , <i>V. uliginosum</i> , <i>V. myrtillus</i> , <i>V. vitis-idaea</i> , <i>O. palustris</i> , <i>E. nigrum</i> , group 3: <i>E. vaginatum</i> , group 4: <i>P. strictum</i> , group 5: <i>P. sylvestris</i> , group 6: <i>P. abies</i> , group 7: <i>B. pendula</i> , <i>B. pubescens</i>	1:0	0.1	0.1	2000	0.974433
S18	Plant-derived; ALK, FA	All; group 1: <i>S. angustifolium</i> , <i>S. magellanicum</i> , <i>S. capillifolium</i> , <i>S. fuscum</i> , group 2: <i>C. vulgaris</i> , <i>V. uliginosum</i> , <i>V. myrtillus</i> , <i>V. vitis-idaea</i> , <i>O. palustris</i> , <i>E. nigrum</i> , group 3: <i>E. vaginatum</i> , group 4: <i>P. strictum</i> , group 5: <i>P. sylvestris</i> , group 6: <i>P. abies</i> , group 7: <i>B. pendula</i> , <i>B. pubescens</i>	1:0	0.1	0.1	2000	0.975875
S19	Plant-derived; ALK, ALC, FA	All; group 1: <i>S. angustifolium</i> , <i>S. magellanicum</i> , <i>S. capillifolium</i> , <i>S. fuscum</i> , group 2: <i>C. vulgaris</i> , <i>V. uliginosum</i> , <i>V. myrtillus</i> , <i>V. vitis-idaea</i> ,	5:1	0.1	0.1	2000	0.968124

		<i>O. palustris</i> , <i>E. nigrum</i> , group 3: <i>E. vaginatum</i> , group 4: <i>P. strictum</i> , group 5: <i>P. sylvestris</i> , group 6: <i>P. abies</i> , group 7: <i>B. pendula</i> , <i>B. pubescens</i>					
S20	Plant-derived; ALK, ALC, FA	group 1: <i>S. angustifolium</i> , <i>S. magellanicum</i> , <i>S. capillifolium</i> , <i>S. fuscum</i> , group 2: <i>Calluna vulgaris</i> , <i>Vaccinium uliginosum</i> , <i>V. myrtilus</i> , <i>V. vitis-idaea</i> , <i>Oxycoccus palustris</i> , <i>Empetrum nigrum</i> , group 3: <i>E. vaginatum</i> , group 4: <i>Polytrichum strictum</i> , group 5: <i>P. sylvestris</i> , group 6: <i>Picea abies</i> , group 7: <i>Betula pendula</i> , <i>B. pubescens</i>	5:1	0.1	0.1	2000	0.967641
S21	Plant-derived; ALK, ALC, FA	group 1: <i>S. angustifolium</i> , <i>S. magellanicum</i> , <i>S. capillifolium</i> , <i>S. fuscum</i> , group 2: <i>C. vulgaris</i> , <i>V. uliginosum</i> , <i>V. myrtilus</i> , <i>V. vitis-idaea</i> , <i>O. palustris</i> , <i>Empetrum nigrum</i> , group 3: <i>E. vaginatum</i> , group 4: <i>P. strictum</i> , group 5: <i>P. sylvestris</i> , group 6: <i>P. abies</i> , group 7: <i>B. pendula</i> , <i>B. pubescens</i>	5:1	0.2	0.1	2000	0.96764
S22	Plant-derived; ALK, ALC	group 1: <i>S. angustifolium</i> , <i>S. magellanicum</i> , <i>S. capillifolium</i> , <i>S. fuscum</i> , group 2: <i>C. vulgaris</i> , <i>V. uliginosum</i> , <i>V. myrtilus</i> , <i>V. vitis-idaea</i> , <i>O. palustris</i> , <i>E. nigrum</i> , group 3: <i>E. vaginatum</i> , group 4: <i>P. strictum</i> , group 5: <i>P. sylvestris</i> , group 6: <i>P. abies</i> , group 7: <i>B. pendula</i> , <i>B. pubescens</i>	5:1	0.1	0.1	2000	0.997097